JOURNAL OF GEOPHYSICS RESEARCH, VOL. 94, NO. D2, PAGES 2303–2320, FEBRUARY 20, 1989

Viewing Zenith Angle Dependence of Cloudiness Determined From Coincident GOES East and GOES West Data

PATRICK MINNIS

Atmospheric Sciences Division, NASA Langley Research Center, Hampton, Virginia

The dependence of observed cloudiness on the satellite or viewing zenith angle (VZA) is examined, using a combination of two cloud amount data sets derived from nearly simultaneous, collocated Geostationary Operational Environmental Satellite (GOES) West and GOES East radiances over the Pacific Ocean during May 1979 and July 1983. A third data set, GOES Prime, is used to estimate the amount of cloud variation due to changes in sensor resolution with VZA. The data are analyzed for single-layer and total cloudiness, as derived with a hybrid bispectral threshold method. The frequencies of occurrence for low, middle, and high clouds, 96%, 47%, and 28%, respectively, are typical of oceanic cloud populations. Cloud fractions increased with increasing VZA for almost all cases. Low clouds showed the greatest increases for small cloud amounts around 0.1, while the greatest increases for high clouds were found for cloud amounts around 0.5. Midlevel clouds showed only a slight dependence on VZA. Total cloudiness increased the most, reflecting its predominantly low-cloud composition. Uncertainties in retrieved cloud fraction also increase with the VZA. Resolution changes with VZA were estimated to cause up to 28% of the increase in cloudiness for certain low-cloud amounts. Very little of the high-cloud increases were the result of resolution changes. Simple geometrical formulas were used to model the results. A single-layer cumulus model was found to be the best fit to the layer cloud data. A formulation combining the single-layer models was used to describe the variation of total cloud cover with VZA. The regression fit of these data to the multilayer model reduced the mean bias errors due to VZA effects from ≈0.058 to ≈0.004. It is concluded that the effects of the VZA should be incorporated in the construction of satellite-derived climatologies and other Earth-observing applications.

1. INTRODUCTION

The analysis of satellite data for the determination of cloud parameters, such as cloud amount, height, and albedo, depends on many variables. These include cloud type and background, the viewing and illumination angles, the spectral ranges and spatial resolution of the measurements, and the algorithm applied to the data. Understanding the relationships of these variables to the derived cloud properties is essential to determining the accuracy and reliability of a given cloud parameter retrieval. Such knowledge is imperative, given the implementation of the International Satellite Cloud Climatology Project (ISCCP), a 5-year global climatology of cloud parameters derived from satellite radiances [*Schiffer and Rossow*, 1983].

The ISCCP is using data from a combination of geosynchronous and Sun-synchronous satellites. Sun-synchronous satellite scanners view a given region at the same local hour each day over a range of viewing zenith angles (for example 0°–70°). If it is assumed that views taken from the zenith yield the true cloud amounts, what are the errors in the monthly mean cloud fraction due to variations in the viewing zenith angle (VZA)? A geosynchronous satellite "sees" a given area from a constant VZA. Cloud amounts derived over one region may be biased relative to the cloudiness inferred over another region, simply because the VZAs are different. For example, the mean cloudiness over one region with VZA = 50° may be 10% higher than that over an area with VZA = 15°. The difference may be real, or it may be only a result of the VZA differences. Such interpretations and error assessments can be made more intelligently if it is known in what manner the derived cloud fraction is affected by the satellite's zenith angle.

It is well known that there is a general tendency to overestimate cloud coverage at high VZAs from satellites or from low elevation angles from the surface. Some of the overestimation of cloud amount from ground observations relative to satellite measurements has been attributed to this effect [*Malberg*, 1973], since the cloud cover estimated from the ground is derived from a combination of high and low elevation angles. *Lund and Shanklin* [1973] estimated the probabilities of cloud-free lines of sight from whole-sky photographs taken over Columbia, Missouri. Their results showed that the elevation angle (90° − VZA) dependence of cloud-free lines of sight varied with cloud type and the amount of sky cover, but decreased with decreasing elevation. This effect is the complement of increasing cloud cover with increasing VZA.

Vemury et al. [1984] were able to attribute much of the albedo differences between the Nimbus 7 Earth Radiation Budget (ERB) scanners and wide field of view radiometer to a systematic increase in the selection of cloudy scenes with increasing satellite zenith angles. That study clearly demonstrated an increase in cloud amount with increasing viewing zenith angle and its impact on albedo. It provided little information, however, on the variation of this relationship for different cloud conditions and cloud types. *Bunting and Hardy* [1984] presented the results of a study by the U.S. Air Force, which showed a negligible change in oceanic cloudiness derived from VIS data taken at VZAs between 0° and 45°. The same data reveal a rapid increase in total cloud cover with increasing VZA for satellite zenith angles between 45° and 78°. Cloud cover derived with IR data taken at the same time show a slightly different variation with VZA. *Snow et al.* [1985] used a very limited set of cumulus cloud photographs, taken from the space shuttle as it approached

Paper number 88JD04001.

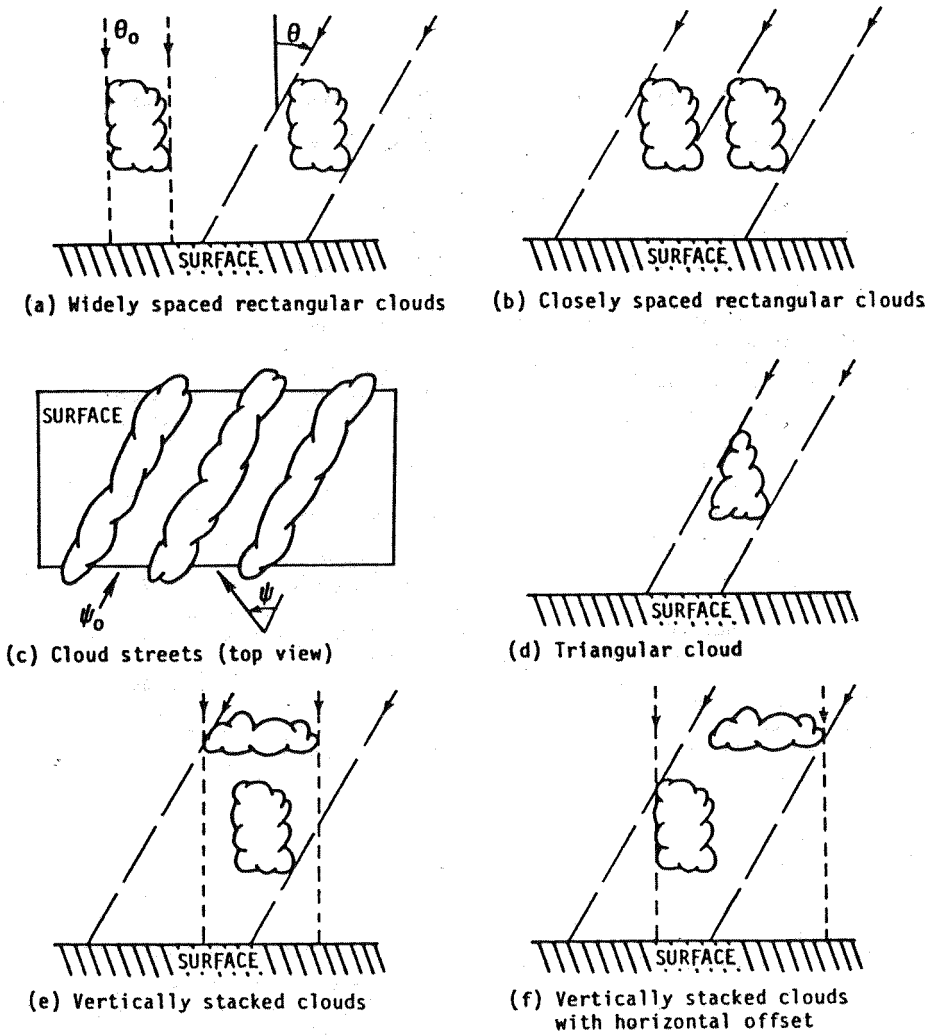

Fig. 1. Illustration of viewing zenith angle effects for various cloud field configurations.

and passed by specific target sites, to determine the apparent cloud amount as a function of VZA. While that study is one of the first to study VZA effects on observed cloud cover using data taken nearly simultaneously over the same area from various VZAs, it does not adequately address the VZA question with respect to the ISCCP and other similar automated satellite cloud retrieval systems. For example, the ISCCP will utilize a bispectral threshold algorithm [*Rossow et al.*, 1985] on a global scale, covering all cloud types at 3-hourly intervals.

Because of their locations at 75° and 135°W and half-hourly sampling, the Geostationary Operational Environmental Satellite (GOES) East and West satellites, respectively, offer conditions for observing the same areas nearly simultaneously with the same type of instrumentation at different viewing (satellite) zenith angles. In this paper a hybrid bispectral threshold method is applied to collocated visible and infrared data from these two satellites to derive the changes in cloud fraction with VZA for various combinations of cloud amounts and heights. The results are used to examine the relationships between cloudiness and VZA and to determine a means for correcting the cloud amounts for any biases which may result from that dependency.

2. Factors Affecting VZA Dependence of Observed Cloud Amount

2.1. *Viewing Perspective*

It is assumed that true cloud cover over a given area is that fraction of the area at the surface which is covered by clouds, as seen from the zenith. The apparent cloud amount over this same area observed from angles off the zenith will not always be the same as the true cloud amount. One reason for this variation of apparent cloud cover with VZA for a visual observer or for a radiatively based computer algorithm is the effect of foreshortening. This effect is related to the vertical extent of the clouds in the field, their spacing, orientation, and shapes. Some simple examples of these variables and their effects are shown in Figure 1.

Figure 1*a* shows a schematic cross-section of two identical clouds having width, x, length, y, and thickness, z, and their areas, C_0 and C, projected on the surface for viewing zenith angles of $\theta_0 = 0°$ and θ, respectively, viewed perpendicular to their lengths. The quantity C_0 is the fraction of some arbitrary area, A, which is covered by clouds, or $C_0 = xy/A$. In this case, the apparent cloud amount is

$$C = C_0(1 + (z/x) \tan \theta)$$

because there is no interference by one cloud with the line of sight to another cloud. The horizontal spacing between these two clouds is reduced in Figure 1*b* such that the gap between them is no longer visible at θ. Thus when the gap width is less than $z \tan \theta$, the clear line of sight at θ between the clouds disappears, and the apparent cloud fraction decreases. If the view to the y face of the cloud is not perpendicular, then the apparent cloud fraction can be expressed in the more general form,

$$C = C_0(1 + \beta \tan \theta)^{\gamma} \quad (1)$$

where $\beta = z/w$ and the horizontal dimension along the observing azimuth, ψ, is $w = x \sin(\psi - \psi_0) + y \cos(\psi - \psi_0)$. The variable γ is defined as the cloud-masking exponent and will be explained later. The angle ψ_0 defines the orientation of the clouds. For a cloud field having a definite orientation, the apparent cloud cover at θ will depend on the azimuth angle of the view. An extreme example of such an effect is illustrated in the idealized cloud streets in Figure 1*c*, where the cloud field consists of long parallel blocks passing completely through some finite region defined by the solid line. If the line of sight is parallel to the cloud orientation (that is, $\psi = \psi_0$), then β becomes very small and, essentially, $C = C_0$ independent of θ.

Many clouds are not shaped like rectangular solids; they may have rounded sides and tops. For example, Figure 1*d* shows a schematic cloud which has the same vertical and horizontal dimensions as that in Figure 1*a*, except that the top is rounded rather than rectangular. In this instance, it may be seen that the apparent cloud area at θ is less than that of its rectangular cloud counterpart. Vertical arrangement of the cloud field may also cause some variation of the VZA dependence of C. The example given in Figure 1*e* yields an effect similar to that in Figure 1*a*. The upper cloud layer acts as a vertical extension of the lower cloud. If the upper cloud is moved, as in Figure 1*f*, then conditions may arise such that $C_0 > C$.

2.1.1. *Single-layer models.* Some of the possible scenarios for single-layer cloud fields may be formalized using the idealized relationships between C and C_0 given by *Snow et al.* [1986]. The rectangular solid model schematized in Figure 1*a* is described with (1). Cloud shape effects may be simulated with spherical,

$$C = C_0(sec\ \theta)^{\gamma} \quad (2)$$

or hemispherical dome,

$$C = C_0\{(1 + \sec \theta)/2\}^{\gamma} \quad (3)$$

or domed cylinder models,

$$C = C_0\{(1 + \sec \theta + B \tan \theta)/2\}^{\gamma} \quad (4)$$

among others. The parameter B is the resultant height-to-width ratio accounting for both the cylindrical and hemispherical portions of the cloud. A special case of (4) is the single-layer cumulus model,

$$C = C_0\{(1 + \sec \theta + \theta \tan \theta)/2\}^{\gamma} \quad (5)$$

where B is replaced by the VZA and θ is in radians. This formulation was originally developed by *Snow* [1986]. To account for interference by one cloud with the line of sight to another cloud, as illustrated in Figure 1*b*, the parenthetical arguments in (1) through (5) are raised to the γ power, where $0 \leq \gamma \leq 1$. No cloud masking occurs at $\gamma = 1$. More details of the derivation of these models are found in the appendix. Obviously, cloud type is an important determinant in the values of either β or γ. Stratiform clouds will be thin relative to their horizontal dimensions and less cellular than more vertically developed cumulus clouds. It is likely that the values of γ and β will be greater for the latter cloud type.

2.1.2. *Total or multilayer cloudiness.* Total cloud cover as defined by *Minnis et al.* [1987], hereafter referred to as MHG, is

$$C_1 = C_2 + C_3 + C_4 \quad (6)$$

where the subscripts 1, 2, 3, and 4 refer to total, low ($h < 2$ km), middle, ($2 < h \leq 6$ km), and high cloud cover ($h > 6$ km), respectively, and where h refers to the cloud-top altitude. Each term on the right-hand side of the equation refers to the single-layer cloud fraction which is actually observed by the satellite. The total cloud cover viewed from the zenith includes only those clouds which are seen by the sensor and not obscured by higher clouds, as illustrated in Figure 1*e*. As the VZA increases, the total cloud fraction will change according to the cloud layers present and their coverage and relative positioning. To account for the VZA dependence of C_1 for various mixes of cloud layers, a more general formulation of (6) is required. It is assumed that the observed cloud amount in each layer has some functional dependence on VZA in the absence of overlying clouds. That is, $C_k = C(\theta)_k$ and $k = 2, 4$. Furthermore, it is assumed that these dependencies are the same when higher clouds are present, except that some of the potential change in the lower layer cloud fraction is altered either as a result of exposure or of obscuration by upper level clouds, as illustrated in Figures 1*e* and 1*f*. Thus

$$C_1 = C(\theta)_1 = C[C(\theta)_2, C(\theta)_3, C(\theta)_4, \rho(\theta)_{lh}]$$

where the probability of obscuration of a lower cloud field by a higher cloud deck is

$$\rho_{lh} \propto C(\theta)_l C(\theta)_h f(\theta)$$

The subscripts l and h refer to lower and higher cloud layers, respectively. The function $f(\theta)$ accounts for the change in cloud amount with VZA due to the effective aspect ratio of the vertically extended cloud field. In this study, $f(\theta) = \tan \theta$.

Combining these elements gives the more general formula for total cloud cover:

$$C_1 = \sum_{k=2}^{4} C(\theta)_k + \{b_1 C(\theta)_2 C(\theta)_3 + b_2 C(\theta)_2 C(\theta)_4 + b_3 C(\theta)_3 C(\theta)_4\} \tan \theta \quad (7)$$

The constants of proportionality are b_i, $i = 1, 3$. If the upper cloud layer obscures the lower layers as θ increases, then $b_i < 0$.

2.2. *Algorithm Effects*

Other variables may also affect the VZA dependence of C from automated satellite cloud retrievals. For example, if bidirectional reflectance is an important part of the cloud

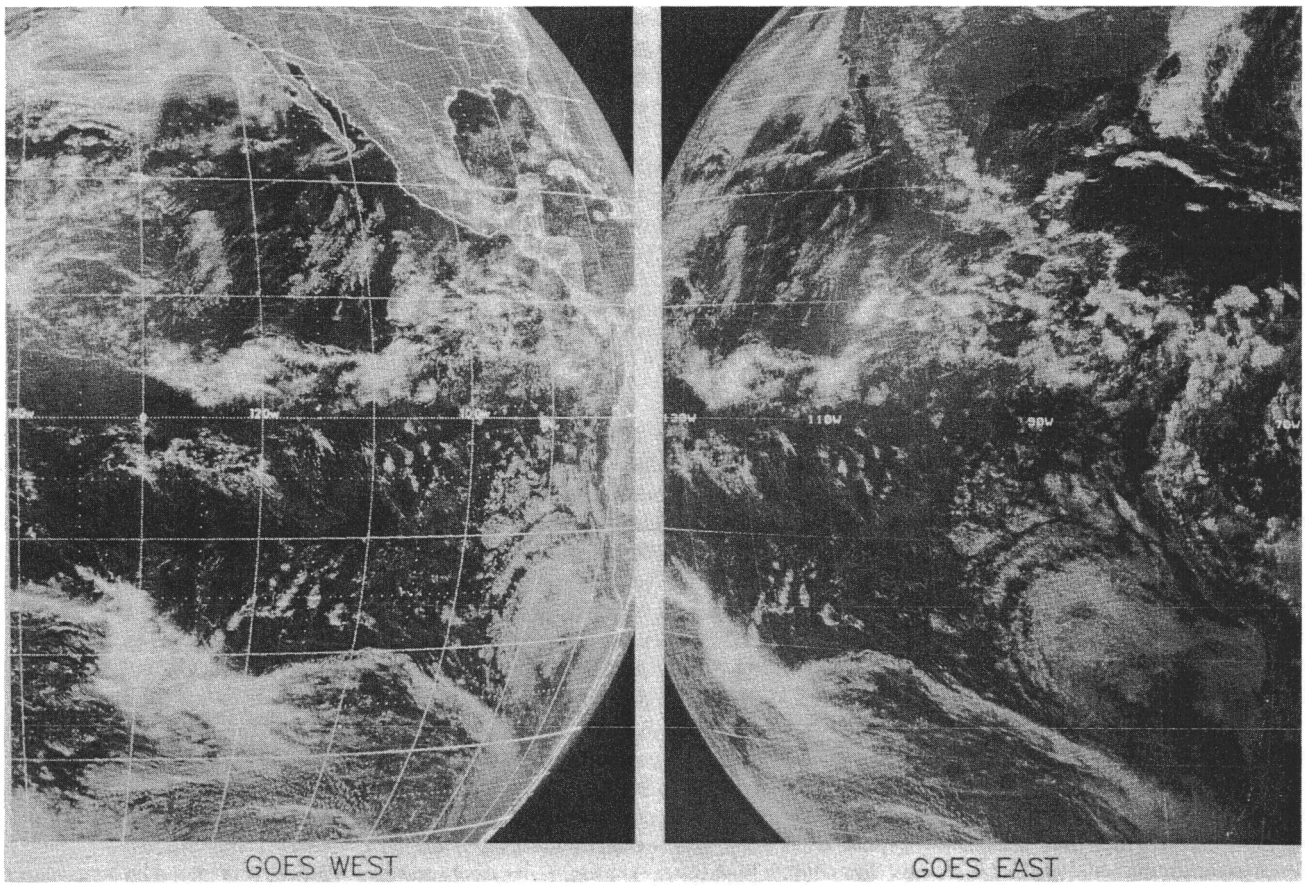

Fig. 2. Nearly simultaneous views of the eastern Pacific, 2100 UT, May 14, 1979.

analysis algorithm, then any biases or random errors in the bidirectional model which depend on the viewing zenith and azimuth angles may be reflected in the retrieved cloud fraction. In a similar vein, the accuracy of the estimate of the clear-sky radiance may depend on the viewing angle affecting the value of the cloud/no-cloud threshold used in threshold methods.

Another possible cause for an increase in apparent cloud amount with increasing VZA is the change in the areal resolution of the sensor's field of view with varying VZA. *Shenk and Salomonson* [1972] demonstrated that cloud amount retrieved with a single threshold method will always increase for true cloud amounts less than 0.5 whenever the ratio of the sensor field of view size to areal cloud size decreased past a critical value. While their results are not expected to be totally applicable to all threshold methods resolution effects should be taken into account when studying the dependence of cloud amount on VZA.

From this discussion it is apparent that the VZA dependence of cloud fraction retrievals from space depends on many variables which may either act together or cancel each other. A complete theoretical treatment of the problem is prohibitive at this point in time. Thus an observational analysis is performed here to gain some quantitative understanding of how the hybrid bispectral threshold method's derived cloud amounts depend on the satellite zenith angle. The analysis will determine which idealized single-layer cloud model and resulting values of γ or β best describe the observations. The single-layer models will then be used with the total cloud amount observations to estimate the coefficients, b_i. An empirical analysis will also be performed to determine to what extent resolution changes affect the VZA dependence of observed cloud cover.

3. DATA

In this study, total, low, middle, and high cloud amounts were derived over ocean regions from two sets of nearly simultaneous GOES East (centered at 75°W and designated GE) and GOES West (centered at 135°W and designated GW) visible (0.65 μm) and infrared (11.5μm) data, using the hybrid bispectral threshold method (HBTM) described by MHG. The GOES East takes a full-disc image each half hour, beginning on the hour (UT). GW images start 15 min before and after each hour. GOES West data taken 15 min before the hour (UT) are compared to GE data taken on the hour. Thus the data taken by one satellite are separated by 15 min from those taken by the other satellite. A third data set, taken by the GOES Prime satellite centered near 108°W, was also analyzed in order to estimate the effects of changing field of view sizes with varying VZAs.

3.1. *May 1979 8-km Data*

The first of the two data sets consists of 11 hours of 8-km resolution daylight data (1700 through 2300 UT) obtained between May 10 and May 15, 1979. An example of a pair of images from this data set is shown in Figure 2 for 2100 UT May 14, 1979. Note that GOES West views down many of the trade wind cloud streets, while GOES East views across them. This set was analyzed on a 2.5° × 2.5° latitude-longitude grid, which includes the ocean areas within the

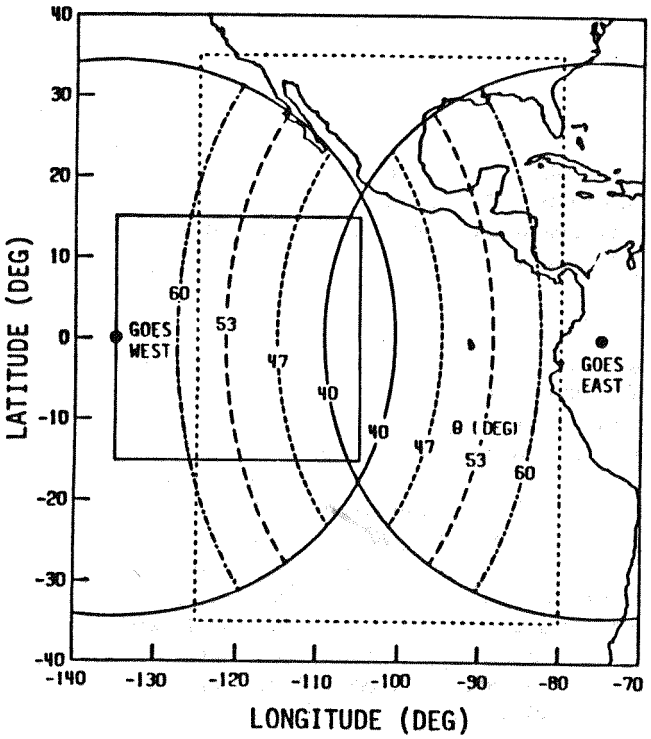

Fig. 3. Areas included in the viewing zenith angle analysis (spring 1979, dashed curve; July 1983, solid curve).

dashed box in Figure 3. Each pixel was navigated as in the work by *Minnis and Harrison* [1984*a*], hereafter referred to as MHa, and assigned to its respective 2.5° region to create the two-dimensional, visible and infrared histograms used by the HBTM. The GE and GW satellites during that time period were SMS 2 and GOES 3, respectively. An intercalibration was performed to normalize the radiances between the two satellites. This calibration consists of a regression on a set of collocated 2.5° × 2.5° regional average visible (VIS) counts and infrared (IR) temperatures. The GE and GW data for regions within 5° of 105°W were taken at 1900 and 1845 UT, respectively. These times are very close to local noon at 105°W, so that each satellite views those regions straddling 105°W at approximately the same solar zenith, viewing zenith, and relative azimuth angles, thereby minimizing the effects of bidirectional reflectance differences, GOES West VIS data were adjusted to match the illumination conditions of the GE data by a simple normalization of the cosines of their respective solar zenith angles.

The result of the linear regression, shown in Figure 4*a* with the VIS data, is

$$D_W = 1.002\ (D_E + 1.114)$$

where D is the VIS digital brightness count between 0 and 63 and the subscripts E and W refer to GE and GW, respectively. The correlation coefficient is 0.996. VIS-reflected radiance is proportional to the square of D. The IR data were found to be related by

$$T_W = 1.007\ (T_E - 3.33)$$

where T is the equivalent blackbody temperature in Kelvins. The correlation coefficient for this regression is 0.998. These preliminary estimates of the SMS 2/GOES 3 intercalibrations are based on 29 data points and are expected to be valid only for the April–May 1979 time period.

Derivation of cloud cover from the GOES VIS and IR data with the HBTM requires an estimate of the VIS counts corresponding to the clear-sky and mean climatological cloud reflectances for a given background and viewing and illumination conditions. The approach taken here follows that of MHG. It uses empirical models of broadband shortwave albedo and bidirectional reflectance anisotropic factors to estimate the reflected broadband radiance, L_{sw}, for clear-sky or mean cloud conditions over ocean for any viewing and illumination situations. The VIS count corresponding to L_{sw} may be found from an empirical relationship described by *Minnis and Harrison* [1984*b*]:

$$L_{sw} = a_0 + a_1 D' + a_2 D'^2 \tag{8}$$

where $D' = (D^2 - D_0^2)^{1/2}$ and D_0 is the offset count for the VIS channel. The coefficients are found through multiple regression between nearly simultaneous collocated and coangled GOES VIS counts and available broadband shortwave (0.2–4.8 μm) radiances. GE VIS counts and L_{sw} data from the Nimbus 7 ERB scanner [see *Jacobowitz et al.*, 1984], taken between April 21 and May 15, 1979, over ocean, were used to determine the coefficients in (8) for this first data set. The results of this regression, shown in Figure 4*b*, are, for $D_0 = 2$,

$$a_0 = 0.0; \qquad a_1 = 1.07; \qquad a_2 = 0.103$$

The correlation coefficient is 0.96. An overhead Sun albedo of 0.07 was used to compute values of L_{sw} from the normalized reflectance models.

3.2. *July 1983 32-km Data*

The second set of cloud amounts was derived from the 3-hourly ISCCP GE (GOES 5) and GW (GOES 6) B2 data. These data consist of navigated, 8-km VIS counts and IR temperatures sampled every fourth scan line and pixel to yield an effective resolution of 32 km. Since these data were sampled, there is no resolution degradation, although there

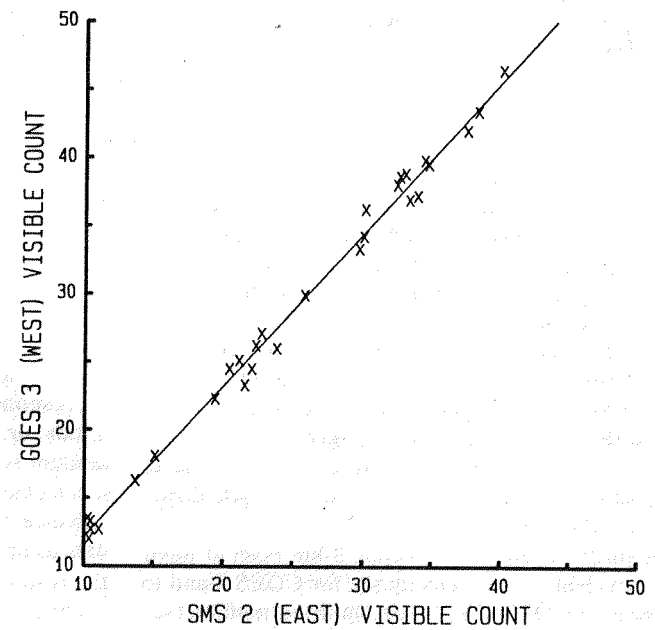

Fig. 4*a*. Correlation and regression line of SMS 2 and GOES 3 visible counts for May 1979.

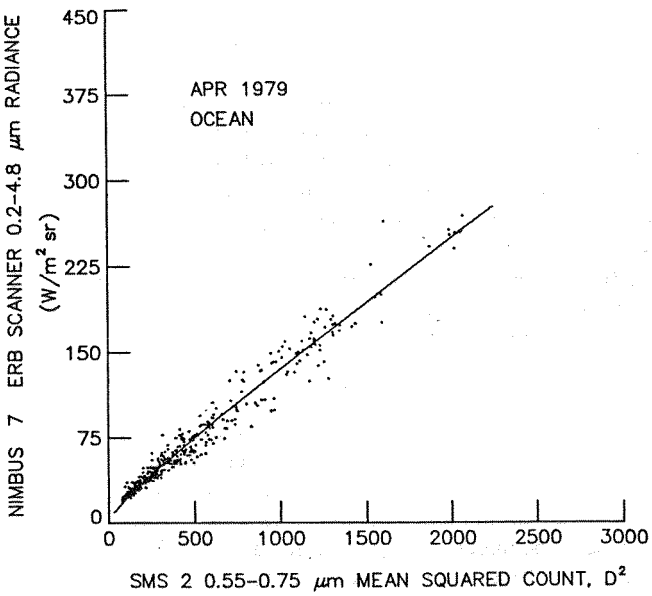

Fig. 4*b*. Correlation and regression curve of SMS 2 visible counts and Nimbus 7 ERB shortwave radiance for April 1979.

is a factor of 16 reduction in the number of pixels per region relative to the May 1979 data. The GE and GW pixels probably do not cover exactly the same areas as a result of this sampling. Cloud parameters were derived from these data for July 17–31, 1983, on a 2.5° × 2.5° grid for the area between 15°N and 15°S and 135° and 105°W, as outlined with the solid box in Figure 3. The GE data were analyzed in the same manner as the GW data described by MHG. The GE VIS calibration is equivalent to the GW calibration (W. B. Rossow, personal communication, 1986). The GE IR temperatures were found to be ~2 K colder than the GW temperatures for the same regions measured at the same angles and times. Since the middle- and high-cloud threshold temperatures depend on the measured clear-sky temperatures, no attempt was made to correct for the calibration differences. The clear-sky temperature limits used for the GE data, however, were set at temperatures 2 K lower than those for the GW data.

3.3. *GOES Prime Data*

Cloud amounts were derived from GOES Prime (GOES 6) 3-hourly, 8-km VIS and IR data taken on April 4 and 14, 1985. The data were first analyzed on a 32 × 32 equal-pixel grid, with 256 regions between ~10°N and 40°S and ~140° and 80°W. The cloud amounts derived from these 8-km data are designated with the subscript, E (for example, C_{E1}, C_{E2}).

The resolution of this data set was reduced to 16 km by averaging the VIS counts and mean equivalent IR blackbody temperatures of the four 8-km pixels in each pair of columns and rows in the 512 × 512 pixel data set to create a 256 × 256 set of VIS and IR pixel pairs. These averaged data were then analyzed with the HBTM on a 16 × 16 equal-pixel grid to create a degraded resolution cloud amount data set, designated with the subscript S.

Neglecting pixel overlap, the nominal 8-km pixel at nadir is actually equivalent to a 6.4-km square for GOES 3 and to a 6.3-km square for GOES 6. Using an empirical method (see appendix), it was determined that the area of the pixel may be approximated in square kilometers as

$$A = 54.4 \sec\theta - 13.8 \tag{9a}$$

and

$$A = 50.7 \sec\theta - 10.3 \tag{9b}$$

for GOES 3 and GOES 6, respectively, for $\theta < 72°$. For these data the mean VZA is ≈20°. From (9*b*), $A(\theta = 20°) \approx 44$ km^2. The fourfold increase in area due to the resolution degradation is therefore equivalent to $\theta \approx 74°$.

4. ANALYSIS METHOD

The spring 1979 and July 1983 results were combined, yielding, after filtering, 7468 regional pairs of cloud amount sets, each having VZAs θ_n and θ_f. The subscripts n and f refer to near-zenith and off-zenith, respectively. A cloud amount set consists of values for C_k, $k = 1, 4$. Near-zenith is described as $\theta < 41°$, while off-zenith corresponds to $\theta \geq 41°$. Figure 3 shows lines of equal VZA for each satellite. Because of the satellite configurations, θ_n and θ_f are fixed for a given region and the value of θ_n decreases, in general, as θ_f increases. The azimuths relative to the Sun, ψ_n and ψ_f, are also nearly constant at a given hour during the month. Thus during the course of a day, only a few solar azimuths are sampled over a specific region.

To minimize any potential azimuthal dependencies and to cover a variety of cloud conditions, the data were organized and averaged as follows: Each pair of cloud amount sets was sorted and summed into off-zenith angular, near-zenith cloud amount bins, and cloud type (for example, total or low), denoted with the subscripts i, j, and k, respectively. There are five categories of near-zenith cloud cover, defined by 0.2 intervals of cloud amount. The off-zenith angular bins are given by

$$i = 1\text{: } 41° \leq \theta_f < 45.6° \qquad i = 2\text{: } 45.6° < \theta_f < 53.1°$$

$$i = 3\text{: } 53.1° < \theta_f \leq 60° \qquad i = 4\text{: } 60° < \theta_f < 71°$$

The angles defining these bins correspond roughly to the lines of constant θ in Figure 3.

Mean near-zenith cloud amounts and angles were computed for each category from the data as follows:

$$\bar{C}(\bar{\theta}_n)_{ijk} = \sum_{l=1}^{N} C(\theta_n)_{ijkl} / N_{ijk} \tag{10}$$

where

$$(\bar{\theta}_n)_{ijk} = \cos^{-1}\left(\sum_{l=1}^{N} \cos\theta_{nijkl} / N_{ijk}\right) \tag{11}$$

and N_{ijk} is the number of cloud amount pairs in category ijk. Mean quantities were computed in a similar fashion for the corresponding off-zenith cloud amounts. The standard deviations, σ, of the differences between each pair of cloud amount sets was computed to estimate the variability of the mean change in cloud amount for a given change in VZA. To enhance the statistical reliability while retaining as much data as possible, all mean cloud amounts were removed from the results if $N \leq 5$ or $\sigma/\sqrt{N} \geq 0.03$.

Only data taken at solar zenith angles less than 81° were used in this study. Data pairs containing total cloud amounts < 0.005 (~2.5% of the total) were eliminated. The remaining

data were filtered for obvious navigation and extreme misclassification errors by removing all data pairs having $C(\theta_f)_1 - C(\theta_n)_1 > 0.45$ and $C(\theta_f)_1 - C(\theta_n)_1 < -0.25$. This somewhat crude filter removed about 3% of the data. Its asymmetric constraints were established by combining an assumed mean VZA bias of 0.10, a maximum $\sigma = \pm 0.18$ computed from an initial processing of the data, and an error of ± 0.17, resulting from potential navigation errors as great as a three-pixel shift (for an overcast region surrounded by clear regions). This filter had little effect on well-sampled bins, but its eliminated a few sparsely sampled bins from the results.

A single-layer cloud field is defined here as a layer containing clouds with no significant cloudiness above it. Thus additional limits were set arbitrarily for the acceptance of single-layer cloud amounts, in order to minimize interference by clouds higher than the specified cloud layer. For midlevel clouds, $C(\theta_n)_3$ is used only if

$$C(\theta_n)_3 / \{C(\theta_n)_3 + C(\theta_n)_4\} > 0.99$$

Low clouds are accepted only if

$$C(\theta_n)_2 / C(\theta_n)_1 > 0.99$$

These constraints allow a maximum of 0.01 detected cloud cover above the specified cloud layer. Although there may be some upper level cloudiness misclassified as lower level clouds because of partially filled pixels, these limits should minimize their influence on lower level cloud amounts.

4.1. *Model Analysis*

4.1.1. *Single-layer cloud fields.* If there is a VZA dependency in C between θ_0 and any other θ, then it is probable that the near-zenith mean cloud amounts computed for angular bins $i = 1, 4$ for a given cloud amount range do not necessarily correspond to the same cloud fraction at θ_0. On the basis of the slight change in cloudiness with θ for $\theta < 40°$ in this (as will be seen in section 5) and other studies [e.g., *Snow et al.*, 1986], it is assumed that the true cloud amounts are sufficiently close that the VZA relationships to cloudiness for $i = 1, 4$ are nearly equal for all $\bar{\theta}_n$. It is possible, then, to estimate the VZA dependency of cloud cover for a given cloud amount and type by determining the mean relationship of C to θ for all four angular bins. The dependencies are derived in terms of the simple models given by (1)–(5), since $\bar{C}(\bar{\theta}_n)_{ijk}$ and $\bar{C}(\bar{\theta}_f)_{ijk}$ should be equal at θ_0.

For example, from (2)

$$\bar{C}_{0_{ijk}} = \bar{C}(\bar{\theta}_n)_{ijk} / \sec^{\gamma}(\bar{\theta}_n)_{ijk} \tag{12a}$$

and

$$\bar{C}_{0_{ijk}} = \bar{C}(\bar{\theta}_f)_{ijk} / \sec^{\gamma}(\bar{\theta}_f)_{ijk} \tag{12b}$$

As suggested by *Snow et al.* [1986], the logarithms of (12) can be rearranged to yield

$$\gamma_{ijk} = \ln [C(\theta_n)/C(\theta_f)] / \ln [\sec \theta_n / \sec \theta_f] \tag{13a}$$

The masking exponent is determined in a similar fashion for all of the other models given by (2) through (5). Setting $\gamma = 1$, the effective aspect ratio in (1) may be given by

$$\beta_{ijk} = \{[C(\theta_n) - C(\theta_f)] / [C(\theta_f) \tan \theta_n - C(\theta_n) \tan \theta_f]\} \tag{13b}$$

The indices and overbars have been omitted in (13) for clarity.

A mean masking exponent,

$$\bar{\gamma}_{jk} = \sum_{i=1}^{4} \gamma_{ijk} N_{ijk} / \sum_{i=1}^{4} N_{ijk}$$

or aspect ratio, is then computed for each cloud type and cloud amount category. The mean cloud amounts at zenith are then computed for the near-and-off-zenith cloud fractions from each cloud amount pair, using each model and its corresponding value of $\bar{\gamma}_{jk}$. The mean and rms differences between the pairs of zenith cloud amounts normalized to the average predicted zenith cloud amounts are computed for each category jk and used to assist in the evaluation of the models. The values of $\bar{\gamma}_{jk}$ for the selected model are then used to graphically estimate $\bar{\gamma}_k$ for all cloud amounts.

4.1.2. *Total cloudiness.* The selected single-layer model is substituted into (7) yielding a more explicit formula for total cloud cover. The coefficients, b_i, are determined by multiple regression on the individual pairs of near-zenith and off-zenith total cloud amounts which are comprised of more than one layer. Thus remaining individual layer cloud amount pairs which were not used in determining values of γ_k, for $k = 2, 4$, in section 4.1.1 are included in this analysis. In order to perform the regression, it is necessary to assume that the interlayer obscuration is negligible for the near-zenith VZAs. This enables the determination of single-layer cloud amounts at θ_0 from the near-zenith, single-layer cloud amounts. The values of $C(\theta_f)_1$ are regressed with the corresponding values of $C_{0_k}(k = 2, 4)$ derived from the near-zenith, single-layer cloud amounts.

4.2. *Resolution Effects*

The contribution of degrading resolution to the change in cloud amount with VZA is estimated by computing the mean differences between the pairs of C_E and C_S in each category jk, using the values of C_E to determine the cloud amount category. Assuming that the change in cloud amount is linear with pixel area, the average change in cloud cover for a given mean cloud amount pair, $\bar{C}(\bar{\theta}_n)_{ijk}$ and $\bar{C}(\bar{\theta}_f)_{ijk}$, due to change in resolution is

$$\Delta C_{Rijk} = P_{jk} \bar{C}(\bar{\theta}_n)_{ijk} \{A(\bar{\theta}_f) - A(\bar{\theta}_n)\} / \bar{A}(\theta_n) \tag{14}$$

where $P_{jk} = (\bar{C}_{Sjk} - \bar{C}_{Ejk}) / 3\bar{C}_{Ejk}$. The factor of 3 in the divisor of this equation is the value of the areal term as given in (14). It represents the fourfold increase in pixel area between 8-km and 16-km GOES data, with the pixel area, A given by (9). The value of the off-zenith cloud amount is then corrected to account for the resolution change by

$$\bar{C}_R(\bar{\theta}_f)_{ijk} = \bar{C}(\bar{\theta}_f)_{ijk} - \Delta C_{Rijk} \tag{15}$$

where the subscript R denotes resolution correction. These corrected quantities are then analyzed with their corresponding values of $\bar{C}(\bar{\theta}_n)_{ijk}$ following these procedures.

4.3. *Other Considerations*

Using different satellites to provide the VZA pairs over a given region introduces the possibility of variations in cloud cover due not only to VZA differences, but also to temporal, azimuthal, and instrumental differences as well as algorith-

TABLE 1. Cloud amounts and differences for Regions Viewed With $|\theta_{GE} - \theta_{GW}| < 5°$

Cloud Type	GOES East Cloud Amount	GOES West Cloud Amount	Mean Difference	rms Difference	Number of Samples
Total	0.528	0.528	0.000	0.069	72
Low	0.308	0.297	0.011	0.067	72
Middle	0.212	0.227	−0.016	0.047	48
High	0.173	0.173	0.000	0.034	33

mic errors. For example, if data from only one region and local time were used in the analysis, the mean difference in near-zenith and off-zenith cloud amounts may be due to a combination of differences in θ, ψ, and time. A region with a regular diurnal cycle of cloudiness will introduce a time bias. Since ψ is relatively constant for a given local time and location and cloud amount may depend systematically on ψ (see section 2), a bias due to ψ may also occur for this region.

Such sources of potential uncertainty cannot be removed explicitly for each region. Thus it is assumed that temporal and spatial averaging of the cloud amounts will eliminate most of the potential biases due to time and azimuthal differences. With averaging, these effects become part of the random uncertainty in the mean cloud amounts in each VZA bin. If the errors from these sources are removed by averaging, then the mean cloud amounts over regions observed by both satellites at the same VZAs should be equal. Thus the cloud amount sets with nearly equal VZAs are differenced to determine if such errors are minimized by averaging.

5. RESULTS

5.1. *Equal VZA*

Table 1 shows the results for regions viewed with $|\theta_{GE} - \theta_{GW}| < 5°$. The mean values of θ for GOES West and GOES East are 36.7° and 37.3°, respectively. In order to obtain a reasonable number of samples, the layer clouds were not restricted in the analysis, as noted in section 4. The mean total and high-cloud amounts for both satellites are equal, while the low- and middle-cloud amounts differ slightly. The total cloud fractions are the same and the low- and middle-cloud differences have opposite signs. It is not likely that the differences arise from the relative positioning of the low–middle cloud temperature threshold in the algorithm. That threshold depends only on the clear-sky temperature observed by the satellite. This small difference, especially for the midlevel cloud fractions, is probably due to the sparse sampling of the July data set. If only the May 1979 data are averaged, this discrepancy disappears. Only 12 of the 48 midlevel cloud amount samples in Table 1 are taken from the July data set. This number may be insufficient to eliminate pixel-sampling deficiencies. Examination of the VZA dependency of midlevel cloudiness, using the data described in section 4, with and without the July data, reveals that the two data sets give essentially the same results. It is concluded that the actual biases in C_2 and C_3 taken from two satellites at the same VZA are negligible.

The rms differences in Table 1 suggest that discrepancies in time, sampling, azimuthal angles, and algorithm inputs

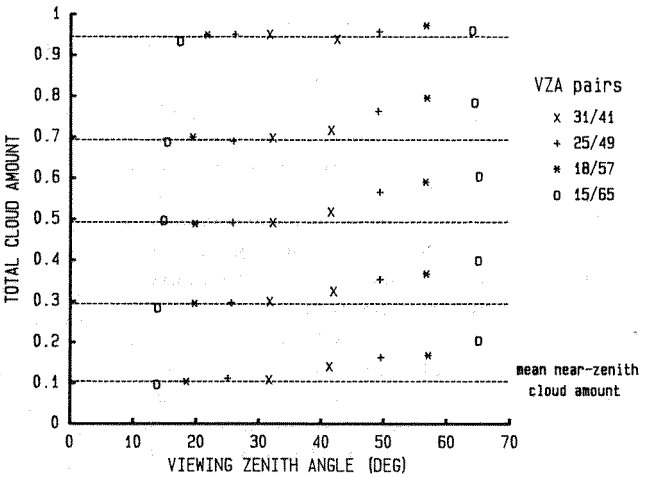

Fig. 5. Variation of mean total cloud cover with viewing zenith angle.

introduce an uncertainty of about ±0.07 in total and low-cloud amounts, a value similar to that found by *Minnis and Wielicki* [1988] for the HBTM. These variables appear to have less effect on the retrievals of middle- and high-cloud amounts. Low-cloud amounts are highly dependent on the analysis of the VIS data, while middle- and high-cloud retrievals are nearly independent of the VIS data. It is expected therefore that estimations of low cloudiness are more sensitive to azimuthal variations in bidirectional reflectance than higher clouds. If it is assumed that there is no azimuthal dependence for the higher clouds and that low- and high-cloud retrievals suffer the same errors due to temporal, sampling, and algorithmic differences, then it may be inferred that azimuthal differences cause rms undertainties of the order of ±0.050. Uncertainties arising from the other sources are approximately ±0.045.

Although these results were derived for VZAs between 31° and 39°, they suggest that biases due to variables other than satellite zenith angle may be eliminated by averaging over various regions and times. Thus it is concluded that variations in mean cloud amounts taken at different viewing zenith angles may be attributed only to changes in VZA.

5.2. *Mean Cloudiness Versus VZA*

Figure 5 shows the mean total cloud amounts for the four VZA pairs with the mean near-zenith cloud amount for each cloud amount category. Cloud cover at θ_f is greater than its low-VZA counterpart, except in one case for $C(\theta_n)_1 > 0.80$. The greatest increases in C_1 occur for near-zenith total cloud amounts less than 0.80. Total cloud amount differences up to 0.11 are found at the highest values of θ_f, translating to increases of up to 110% for the 0.0–0.2 cloud amount range. The standard deviations of these differences, shown in Figure 6, indicate that the change in cloud cover with VZA becomes more uncertain for a given cloud retrieval as the VZA increases. Partly cloudy scenes produce the greatest uncertainties, possibly due to the effects of increased proportions of partially cloud-filled pixels. The increasing standard deviations may also arise from larger navigational and misclassification errors at high angles and, for the July data, smaller sample sizes. Removal of the more uncertain July data results in slightly lower standard deviations. In view of the large standard deviations, this study will rely only on

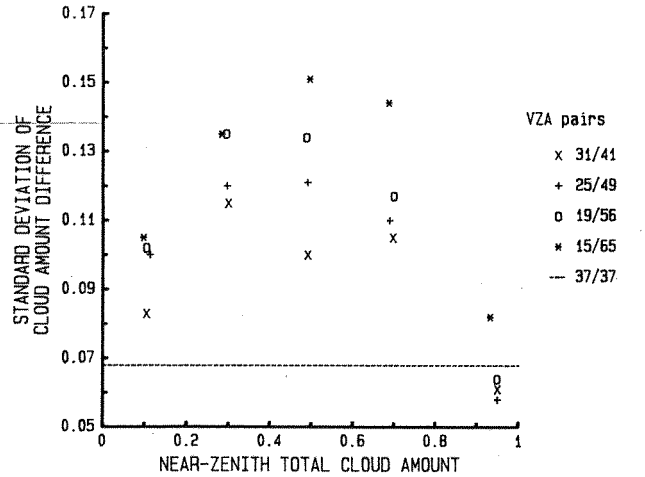

Fig. 6. Variation of mean total cloud amount differences with viewing zenith angle.

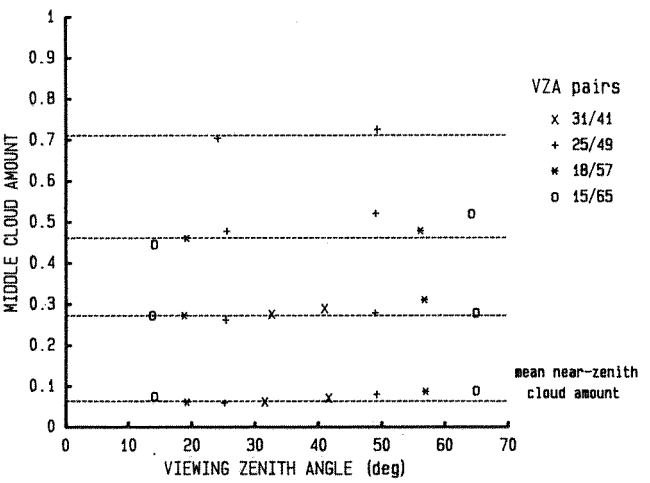

Fig. 7*b*. Same as Figure 5, except for midlevel clouds.

mean cloud amounts to assess the VZA dependence of cloudiness.

The average single-layer cloud amounts are seen in Figures 7*a*–7*c*. Variations in mean low-cloud amounts are similar to those in Figure 5, except for some of the VZA pairs with $C_2 > 0.80$. In those instances, the low-cloud amount actually decreases slightly at the higher VZAs. The increases with VZA are also not as pronounced as those for C_1. Midlevel cloudiness generally increases with VZA, though the changes are significantly less than those found in the low-cloud and total cloud amounts. The erratic data in the $C_3 > 0.4$ categories reflect the poor sampling for some angle pairs. High clouds also increase with VZA for all cloud amounts, except for some pairs with $C_4 > 0.80$. Changes in C_4 with VZA are greater than those seen for the lower cloud layers for cloud amounts between 0.20 and 0.60. The increases in C_4 for angular bin 4 are less than those for bin 3 in the same cloud amount ranges. The standard deviations of the single-layer cloud amount differences increase with VZA like those in Figure 6. Application of the Student t test to these data indicate that for about 75% of the data, the mean differences between the off-zenith and near-zenith cloud amounts are accurate to within ±0.01 cloud cover, at a 90% confidence level. For the remainder of the data, the average 90% confidence interval of the mean values is approximately ±0.02. The less reliable means include the discrepant data noted earlier.

5.3. *Resolution Effects*

The variations of cloud amount with resolution derived from the data described in section 3.3 are plotted in Figure 8 for total and individual layer cloud amounts. Only total and low-cloud amounts between 0.20 and 0.80 seem to be significantly affected by a fourfold increase in the area associated with a GOES pixel. The maximum increase in low and total cloud cover is ~0.07 for $C_{E1} = 0.5$. Midlevel cloud amounts increase by about 0.01 for the same cloud amount category. Very slight decreases occur for small amounts of middle- and high-cloud cover, as a result of resolution degradation. No dependence of the resolution effect on VZA was found for the range of VZAs, $0° < \theta < 45°$, of this data set.

Values for P_{jk} derived from these results are listed in Table 2. The amount of the change in cloud cover for a given change in VZA may be estimated by using these values in (14) and (15) with the results in Figures 5 and 7. The mean changes in observed cloud amount when the VZA is increased from θ_n to θ_f as a result of degraded resolution is

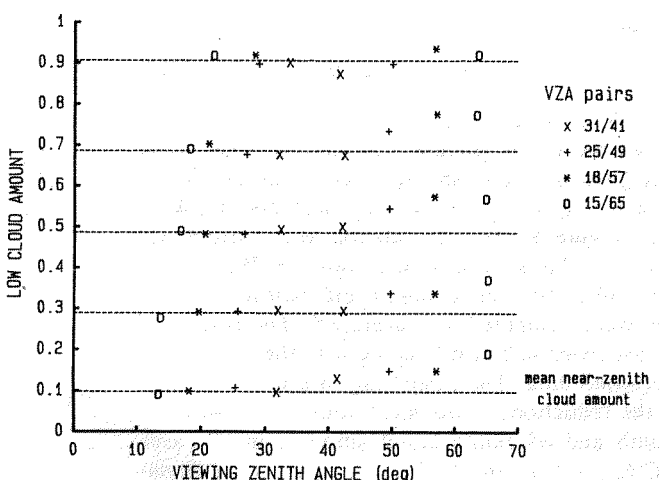

Fig. 7*a*. Same as Figure 5, except for low clouds.

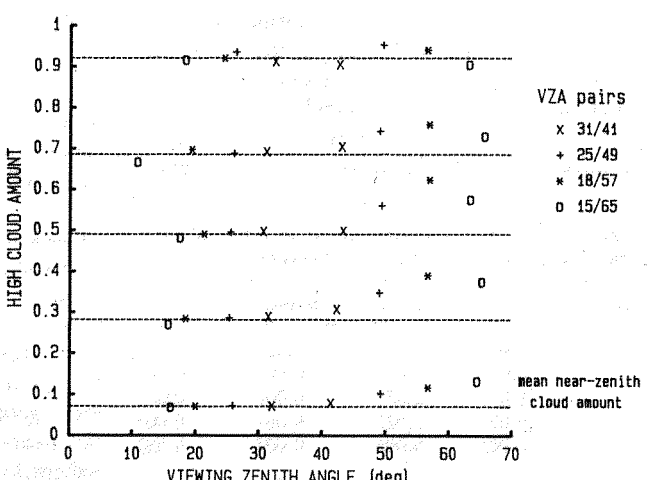

Fig. 7*c*. Same as Figure 5, except for high clouds.

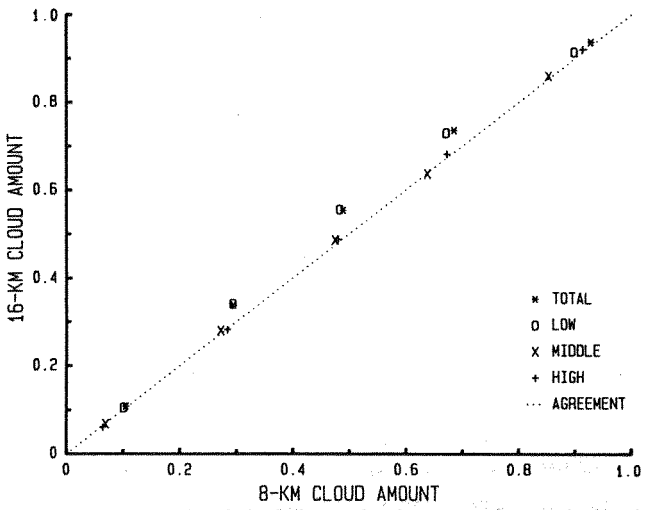

Fig. 8. Mean total and single-layer cloud amounts for nominal and degraded resolution GOES Prime data.

summarized in Table 3. Table 3 was derived by computing the mean differences between the nominal and resolution-corrected off-zenith cloud amounts. The values in parentheses are the percentages of the observed differences between the nominal off-zenith cloud amounts and the corresponding near-zenith cloud amounts which may be attributed to resolution effects. Increases in pixel size account for only a small fraction of the change in cloudiness with VZA for high and middle clouds. On average, the pixel areal changes for the range of VZAs here may account for up to 28% of the observed increases in low-cloud cover. The apparently large effects for cloud amounts greater than 0.8 are insignificant in absolute terms. The changes in total cloudiness reflect the predominance of low clouds in this data set.

5.4. *Model Results*

5.4.1. *Single-layer cloudiness.* From the initial calculations of $\bar{\gamma}$, it was found that the greatest value of $|\Delta\gamma/\Delta C|$ occurs between the first and second cloud amount bins. In order to obtain a better picture of the variation of $\bar{\gamma}$ with small cloud amounts, the data in category $j = 1$ were subdivided into 0.05 intervals of cloud amount. Averages for these subcategories were computed and analyzed, following the procedures described in sections 4.2 and 4.4. All of the resulting values of γ and β for the nominal means, including total cloud cover, are listed in Table 4. The normalized mean and rms differences shown at the bottom of the table were computed only for the single-layer data. "Hemidome" refers to the hemispherical domed cylinder model.

In nearly all cases, the parameters decrease monotonically with increasing cloud amount. Values of $\bar{\gamma}$ are nearly equal

TABLE 2. Relative Change in Observed Cloud Amount per Fractional Change in Pixel Area, GOES Prime Data

Cloud Amount	Total	Low	Middle	High
0.0–0.2	0.015	0.015	−0.016	−0.023
0.2–0.4	0.048	0.053	0.009	−0.004
0.4–0.6	0.043	0.050	0.008	0.005
0.6–0.8	0.024	0.028	0.001	0.004
0.8–1.0	0.003	0.006	0.003	0.002
Number of samples	3275	2280	913	475

TABLE 3. Mean Change in Cloud Amount From θ_n to θ_f Attributed to Pixel Resolution Variation, Where $\theta_n < 40°$ and $40° < \theta_f < 70°$

Cloud Amount	Total	Low	Middle	High
0.0–0.2	0.001(1)	0.002(3)	−0.001(−5)	−0.001(−3)
0.2–0.4	0.011(16)	0.012(25)	−0.001(−5)	−0.001(−1)
0.4–0.6	0.016(21)	0.017(28)	0.002(6)	0.002(3)
0.6–0.8	0.012(17)	0.014(25)	0.000	0.001(2)
0.8–1.0	0.002(22)	0.003(−150)	···	0.001(10)

Percent of total change given in parentheses.

for midlevel cloud amounts between 0.10 and 0.15 and between 0.15 and 0.20. The parameter values range between 0 and 1, except for extremely small cloud amounts. In general, the resolution-corrected masking exponents are similar, but lower than the nominal case exponents. Reduction of the off-zenith cloudiness for resolution effects decreases $\bar{\gamma}$, especially for low clouds.

The hemispherical dome and cumulus models predict zenith cloud fraction differences which are smaller than the remaining models. Since there is only minimal disagreement between those two models in Table 4, it is necessary to use some criterion other than the differences in cloud amounts to determine the "better" model. As noted by *Snow et al.* [1986], one criterion for a realistic model is the requirement that the derivative of cloud cover with respect to VZA equals zero at θ_0. This requirement eliminates the domed cylinder model. The single-layer cumulus model also appears more suitable than the "hemi-dome" model, because it does not require a specification of an aspect ratio parameter and its values of $\bar{\gamma}$ are smaller for cloud amounts less than 0.20. Thus the remainder of the discussion will focus only on the cumulus model, as given by (5).

The values of $\bar{\gamma}_{jk}$ for the nominal cloud amounts are shown in Figure 9 with the graphically determined curves of γ_k which best fit the individual values. The smoothed curves were drawn to ensure that $0 \leq \gamma \leq 2$. Values for the mean masking exponent for the resolution-corrected cloud amounts are plotted in Figure 10. For $C_k > 0.20$, $\gamma_4 > \gamma_2 > \gamma_3$. At smaller cloud amounts, the low-cloud masking exponent is greater than γ_4. The values of the masking exponent for the resolution-corrected cloud amounts, γ_{Rk}, are basically the same as those for the nominal data, except that $\gamma_{R2} < \gamma_2$.

For these data, (5) may be expressed as

$$C_k = C_{0_k}\{(1 + \sec\theta + \theta\tan\theta)/2\}^{\gamma_k} \tag{16}$$

where $k = 2$, 3, or 4. In order to estimate how well this model reduces the cloud amount bias due to VZA, each off-zenith, single-layer cloud amount used in the derivation of γ_k was adjusted to θ_n, using (16) and the masking exponents in Figure 9. This calculation was carried out following the procedures outlined in section 6.4. Differences between these adjusted cloud amounts and their near-zenith counterparts were computed and averaged. The results of this process are listed in Table 5, along with the differences for the unadjusted data. The model appears to fit the data well, given the reductions in the mean differences between the near-zenith and off-zenith cloud amounts in all cases except for $C(\theta_n)_2 = 0.91$ and $C(\theta_n)_3 > 0.6$. Standard deviations of the differences are essentially unchanged. Overall,

TABLE 4. Mean Cloud Masking Exponents and Effective Aspect Ratios for Various Cloud Field Geometries Using Unaltered Data

Cloud Amount	Rectangular β	Spherical γ	Hemisphere γ	"Hemi-Dome" γ	Cumulus γ
			Total Cloud		
0.00–0.05	4.608	2.674	4.648	2.453	2.093
0.05–0.10	2.445	1.503	2.615	1.377	1.175
0.10–0.15	0.632	0.865	1.500	0.793	0.678
0.15–0.20	0.543	0.763	1.330	0.698	0.596
0.20–0.40	0.275	0.471	0.819	0.435	0.369
0.40–0.60	0.200	0.361	0.629	0.333	0.282
0.60–0.80	0.127	0.240	0.419	0.222	0.188
0.80–1.00	0.003	0.005	0.056	0.006	0.005
			Low Cloud		
0.00–0.05	3.650	2.581	4.487	2.363	2.019
0.05–0.10	1.518	1.296	2.253	1.185	1.014
0.10–0.15	0.561	0.780	1.352	0.715	0.612
0.15–0.20	0.447	0.650	1.130	0.595	0.508
0.20–0.40	0.161	0.290	0.498	0.269	0.229
0.40–0.60	0.152	0.277	0.481	0.257	0.217
0.60–0.80	0.092	0.176	0.304	0.165	0.139
0.80–1.00	0.007	0.013	0.023	0.013	0.011
			Middle Cloud		
0.00–0.05	4.691	1.806	3.173	1.651	1.402
0.05–0.10	0.527	0.743	1.298	0.684	0.581
0.10–0.15	0.146	0.362	0.642	0.328	0.279
0.15–0.20	0.127	0.361	0.625	0.332	0.167
0.20–0.40	0.094	0.179	0.314	0.164	0.140
0.40–0.60	0.106	0.204	0.355	0.189	0.160
0.60–0.80	0.042	0.086	0.153	0.077	0.067
0.80–1.00	N/A	N/A	N/A	N/A	N/A
			High Cloud		
0.00–0.05	3.535	1.856	3.250	1.707	1.446
0.05–0.10	0.586	0.958	1.645	0.897	0.758
0.10–0.15	0.487	0.684	1.191	0.635	0.535
0.15–0.20	0.387	0.598	1.040	0.553	0.468
0.20–0.40	0.321	0.528	0.921	0.487	0.413
0.40–0.60	0.172	0.301	0.522	0.280	0.236
0.60–0.80	0.091	0.177	0.310	0.163	0.138
0.80–1.00	0.008	0.016	0.075	0.015	0.013
			Normalized Uncertainty, %		
Mean	−2.4	−1.7	−2.3	−1.3	−1.3
rms	8.4	7.9	9.0	7.3	7.2

β, effective aspect ratio; γ, cloud masking exponent; N/A, Not available.

the mean bias in single-layer cloud amount due to increases in VZA is reduced from 0.042 to 0.000 with the single-layer cumulus model. Similar reductions were found for the model using the resolution-corrected data.

5.4.2. *Total cloudiness.* The parameters in Table 4 could be used to describe the variation of total cloudiness with VZA with a single-layer model. This approach, however, precludes any allowance for variation in the cloud types that make up the observed cloud field. To permit such variations, an approach utilizing (7) is used here. Substituting the expressions for the single-layer clouds into (7) and rearranging yields the model-specific expression for total cloudiness:

$$C_1 = C_{0_2}\{(1 + \sec\theta + \theta\tan\theta)/2\}^{\gamma_2} \cdot (1 + [b_1C_3' + b_2C_4']\tan\theta) + C_{0_3}\{(1 + \sec\theta + \theta\tan\theta)/2\}^{\gamma_3}(1 + b_3C_4'\tan\theta) + C_{0_4}\{(1 + \sec\theta + \theta\tan\theta)/2\}^{\gamma_4} \quad (17)$$

where the primed variables are given by (16). The regression procedures noted in section 4.1.2 were applied to (17), yielding a multiple correlation coefficient of 0.930 with

$$b_1 = -0.154 \qquad b_2 = -0.311 \qquad b_3 = -0.221$$

for the nominal data, using 3930 multilayer cloud amount pairs. Regression on the resolution-corrected data yielded

$$b_1 = -0.171 \qquad b_2 = -0.300 \qquad b_3 = -0.229$$

with a multiple correlation coefficient of 0.927.

As noted earlier, these regressions were performed based on the assumption that the near-zenith layer cloud amounts could be corrected to the zenith condition without accounting for overlap. Use of these initial coefficients in (17) indicates that adjustments of up to 0.04 may be required for $\theta = 30°$. Therefore these coefficients were adjusted from the initial regression values to their final values, minimizing the bias errors as follows. First, the off-zenith cloud amounts were corrected with (17) to θ_n, following the procedures outlined in section 6.4, using the initial values of b_i. Mean

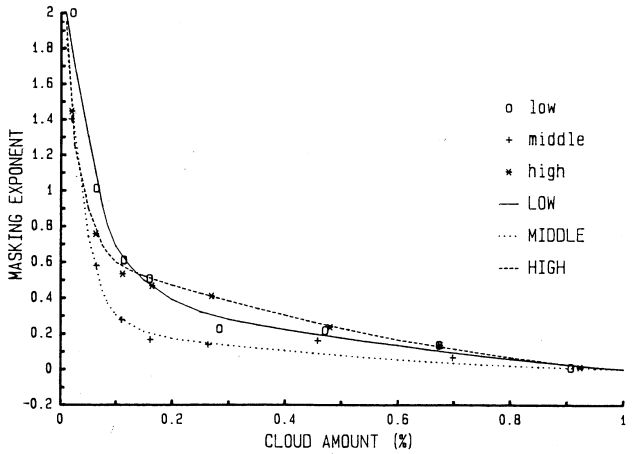

Fig. 9. Masking exponents for single-layer cumulus model, derived from nominal cloud amount data.

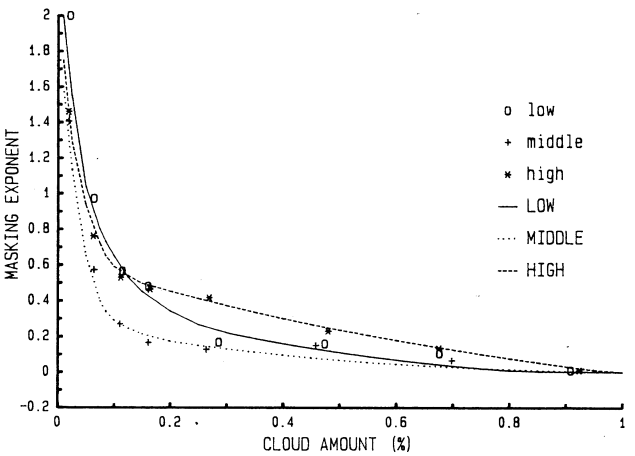

Fig. 10. Same as Figure 9, except for resolution-corrected data.

differences were computed between the corrected off-zenith cloud amounts and the corresponding near-zenith cloud amounts. This procedure was repeated, after adjusting the values of b_i. All data were used in this process, so that lower-layer cloudiness which could be obscured by higher clouds was also included. This iterative procedure was performed until the overall bias in total cloud amount could not be reduced without increasing the overall bias in low- or middle-cloud amounts or until the absolute bias in a given total cloud amount category was less than or equal to 0.02.

Results of this process are listed in Table 6. Values for the final coefficients are

$$b_1 = -0.08 \qquad b_2 = -0.24 \qquad b_3 = -0.14$$

for the nominal data set. For the resolution-corrected data, final coefficients are

$$b_1 = -0.1 \qquad b_2 = -0.28 \qquad b_3 = -0.20$$

The reduction of these coefficients decreased the absolute value of the bias for C_1 in all cloud amount categories. The bias of -0.005 in the model-adjusted mean total cloud amount in Table 6 is smaller than the -0.006 bias found for the adjusted, resolution-corrected data. The greatest biases in the layer cloud amounts occur for $C_2 > 0.8$ and for $C_3 = 0.681$. In both cases a relatively large, though statistically insignificant, positive bias exists before application of the model, a condition which violates the model's basic assumption that cloudiness increases with VZA. The overall reduction in the bias for the layer cloud amounts is not as great as that found for the single-layer cloud amounts in Table 5.

6. Discussion

6.1. *Resolution Effects*

This study provides only a rough estimate of the relationship between the observed cloud amount and sensor resolution. The assumption that the cloud amount varies linearly with effective pixel area may differ from the actual dependence of cloudiness on field of view size. Evaluation of the

TABLE 5. Mean Differences Between Near-Zenith and Off-Zenith Cloud Amounts for Unobstructed Single-Layer Cloud Fields Corrected With Cumulus Model

Cloud Type	$\bar{C}(\theta)_n$	$\overline{C(\theta)_n - C(\theta)_f}$		Standard Deviation		Samples
		Observed	Corrected	Observed	Corrected	
Low	0.099	−0.058	0.002	0.093	0.088	1533
	0.290	−0.047	0.011	0.128	0.128	1091
	0.486	−0.060	−0.011	0.120	0.124	555
	0.686	−0.056	−0.023	0.114	0.126	242
	0.910	−0.002	0.010	0.086	0.087	151
Mean	0.293	−0.052	0.001	0.110	0.110	3572
Middle	0.063	−0.018	0.002	0.064	0.065	1091
	0.270	−0.019	0.004	0.099	0.098	146
	0.468	−0.034	−0.020	0.097	0.110	39
	0.691	0.024	0.033	0.180	0.192	23
	0.916	0.005	−0.012	0.055	0.048	4
Mean	0.112	−0.018	0.002	0.073	0.075	1303
High	0.072	−0.033	0.000	0.063	0.054	1111
	0.285	−0.068	−0.010	0.115	0.113	351
	0.494	−0.067	−0.011	0.109	0.117	220
	0.690	−0.044	−0.003	0.111	0.123	156
	0.924	−0.009	0.001	0.064	0.073	272
Mean	0.306	−0.040	−0.003	0.084	0.083	2110

TABLE 6. Mean Differences Between Near-Zenith and Off-Zenith Cloud Amounts for Total Clouds in Multi-Layer and Single-Layer Conditions Corrected With Interlayer Masking Model

Cloud Type	$\bar{C}(\theta)_n$	$\overline{C(\theta)_n - C(\theta)_f}$		Standard Deviation		Samples
		Observed	Corrected	Observed	Corrected	
Total	0.105	−0.066	−0.005	0.105	0.093	1898
	0.294	−0.067	−0.002	0.126	0.126	1840
	0.492	−0.077	−0.014	0.126	0.132	1363
	0.694	−0.071	−0.014	0.118	0.134	943
	0.949	−0.009	0.010	0.064	0.077	1442
Mean	0.459	−0.058	−0.004	0.109	0.113	7486
Low	0.107	−0.053	−0.007	0.094	0.092	3000
	0.287	−0.042	0.002	0.125	0.128	2461
	0.484	−0.042	−0.003	0.131	0.137	1076
	0.684	−0.035	−0.008	0.125	0.135	406
	0.901	0.012	0.021	0.110	0.118	210
Mean	0.282	−0.045	−0.003	0.114	0.116	7153
Middle	0.084	−0.020	−0.003	0.063	0.065	1857
	0.288	−0.010	−0.009	0.081	0.087	1048
	0.479	0.010	−0.009	0.091	0.100	416
	0.681	0.049	0.021	0.136	0.142	99
	0.901	0.002	−0.008	0.042	0.038	8
Mean	0.214	−0.011	−0.005	0.075	0.080	3428

linear assumption would require a more highly resolved data set in order to simulate several intermediate pixel sizes.

Although the data used to derive the resolution effects differ from the data sets used in the VZA analysis, they are taken from the same geographical area and season as part of the spring 1979 data. Furthermore, the same resolution study was performed using another April 1985 data set, taken over the northeastern Pacific, yielding nearly identical results. It is concluded therefore that the present estimates of resolution effects on the observed cloud cover are applicable to this study.

Correcting the cloud amounts for the VZA directly with the nominal exponents is as accurate as changing the cloud amounts with the resolution-corrected exponents and adjusting for the pixel resolution with the empirical results. Both pixel size and the cumulus model depend on sec θ. Thus the cumulus model implicitly incorporates the resolution effects.

6.2. *Single-Layer Cloudiness*

6.2.1. *Representativeness of the results.* It is apparent from Tables 5 and 6 that low clouds make up the majority of the cloud observations in this data set. They were found in almost 96% of the observations and without significant amounts of higher clouds in 48% of the data. Midlevel and high clouds were observed in 47% and 28% of the results, respectively. There are presently no cloud amount data available to directly compare with these results. The frequencies of occurrence of these cloud types, however, are compared below with climatology to determine if these results are typical of the mix of cloud layers expected over the oceans.

The climatology of occurrence of various cloud types observed from ships produced by *Hahn et al.* [1982], hereafter referred to simply as Hahn, may be used to estimate how often a particular cloud type occurs and how frequently it is found alone. Cumulus, stratus, nimbostratus, and cumulonimbus clouds are classified by Hahn as low clouds, since their bases are at low levels. Altocumulus and altostratus types are defined as midlevel clouds, and all cirriform types are high clouds. Except for nimbostratus, which may also be considered as a middle cloud, the low-cloud types are considered to be mutually exclusive, so that the sum of their probabilities gives the total low-cloud probability. Nimbostratus is classified here as midlevel cloud all of the time and as low cloud half of the time, so it falls into two levels. Data from Hahn are also grouped according to season, so for comparison purposes, it is assumed that a seasonal value represents the months which make up the given season. Approximately half of the data in the present study were taken during May and the other half during July. Thus mean probabilities of occurrence and contingency probabilities for low, middle, and high clouds were computed using Hahn's data from the northern hemisphere spring and summer, averaged over the respective areas given in Figure 3.

From these averages it is estimated that when any clouds are observed, 96% of the time low clouds make up at least part of the cloud cover. High and midlevel clouds are rarely observed alone but are seen about 31% and 49% of the times, respectively, when any cloudiness is reported. Approximately 43% of the cloud observations consist only of low-cloud types, which are mostly either stratus or cumulus. Considering the temporal, spatial, and perspective differences, these percentages are very close to those in the present study. Furthermore, these percentages are within ±2% of the mean occurrence probabilities for all of the mostly ocean regions between 45°N and 45°S in Hahn's spring data set. Because of assumptions required in the ship data analysis resulting from obscuration difficulties, the actual probabilities of low, middle, and high clouds may be slightly different than those reported by Hahn. It is concluded from this comparison, however, that the combinations of cloud types used in the present study are typical of oceanic cloud regimes.

6.2.2. *Parameter variations.* The results in Figures 7*a*–7*c* and Table 5 depict mean cloud amounts and mean near-zenith and off-zenith cloud amount differences and

standard deviations, which generally increase with VZA and which vary considerably with cloud layer. Discounting the effects of changing pixel resolution, the foreshortening discussed in section 2.1 can easily account for most of the increase in mean cloud amount with increasing VZA. The increases in the standard deviations of the mean cloud amount differences may also be explained by the variety of geometric arrangements of cloudiness. For example, a cloud amount of 0.50 may consist of widely spaced small clouds with large vertical aspect ratios or of a single, flat sheet of stratus which covers half of the region. The former would tend to produce large increases of cloudiness as VZA increases, while the latter may yield negligible increases for a 2.5° region. Thus for any rise in VZA, the observed cloud amount may remain the same or increase. Since mean cloud amount increases with rising VZA, the range of individual changes in cloudiness, and therefore the standard deviations, must also increase. The higher standard deviations for $0.2 < C < 0.8$ probably reflect a mix of small clouds and continuous sheets. For nearly and clear overcast conditions, it is likely that widely spaced clouds and stratus clouds are most predominant, respectively, so that the standard deviations are smaller than they are for 50% cloud cover.

This effect of cloud type, cumuliform or stratiform, on the variation of cloud amount with VZA may also help explain why the behavior of the masking exponent changes with the altitude of the cloud layer. Before considering this aspect, it should be noted that while the selected model provides the best fit of those considered, it is not necessarily an accurate physical model of all cloud types. For example, there is no obvious reason why a cirrus ensemble should act like an idealized single-layer cumulus field. The two primary variables governing foreshortening are the effective aspect ratios and the cloud spacing, which together determine the amount of masking. Since there is only one parameter accounting for both effects in the model, any discussion of the behavior of γ must consider both variables which are functions of the cloud types that make up each layer.

Trade cumulus clouds are probably the most predominant low-level clouds in the maritime tropics for $C_2 \leq 0.40$. This cloud type is characterized by ensembles of relatively small ($w < 4$ km), individual cloud elements with significant vertical aspect ratios ($\beta > 0.5$). They often occur in streets separated by 2 to 8 km, with lengths up to 200 km [*Kuettner*, 1971]. Well-separated clouds would yield a value of unity for the masking exponent for most values of θ. Thus for $C_2 < 0.1$ where $\gamma_2 \geq 1.0$ (Figure 9), it is expected that there is little interference by one cloud with another. As cloud amount increases, both cloud spacing and vertical aspect ratios are probably decreasing, until γ_2 levels out at ~0.2 for $C_2 > 0.3$. This may be the result of the average low-level cloud field changing from many small, vertically developed elements to fewer, larger, more flattened cloud cells. The latter are typical of stratocumulus clouds which are more common over the ocean for $C_2 > 0.40$.

The lowest values of γ are found for midlevel clouds. This suggests that they are most likely to occur as relatively thin decks of closely spaced elements, which is consistent with the typical observation of altostratus or altocumulus. Higher values of γ_3 for $C_3 < 0.1$ may be due to vigorous cumulus cells which penetrated the middle layers.

The greatest values of γ for cloud amounts greater than 0.15 are found for high clouds. Generally, the clouds in the upper layer are mainly cirriform or the tops of well-developed cumulonimbus clouds. Because of ice crystal fallout, cirrus tends to have considerable vertical development. The large values of γ_4 indicate that the cirrus cloud fields may contain widely spaced elements with significant vertical aspect ratios, even at cloud amounts greater than 0.5. Cumulonimbus clouds also have large aspect ratios and tend to be widely separated. Because of the large altitude range available for growth, the vertical aspect ratios of upper level clouds can be much greater than the lower clouds. Thus the values of the masking exponents of the high clouds are expected to be greater than those of the lower clouds.

The masking exponent values derived from the data are generally well behaved with respect to the model boundary conditions, except that $\gamma > 1$ for $C < 0.05$ for all cloud types. At such small cloud amounts the value of γ is quite sensitive to small errors. The average value of $\sigma/\sqrt{N}$ for middle and high clouds is 0.004 for mean cloud amounts less than 0.05. This uncertainty translates to a range $1.0 \leq \gamma < 1.7$ for middle and high clouds. From a statistical standpoint the model boundary condition therefore is not necessarily violated by the data for these cloud layers. For low clouds, $\sigma/\sqrt{N} = 0.008$ for $C_2 < 0.05$. If the off-zenith low-cloud amounts are reduced by this amount and γ_2 is assumed to be unity, there still remains a 0.01 bias in the off-zenith data after correction for VZA using the cumulus model. Because of the larger uncertainties in the low-cloud amounts (see Table 1), it is more difficult to assess the statistical significance of such small mean values of C_2. If it is assumed, however, that the remaining bias is statistically significant, then it must be concluded that the model is inadequate for $C_2 < 0.05$ or that the algorithm tends to produce a bias for very little cloudiness, either for small or large VZAs. The other models summarized in Table 4, however, appear to be even less physically realistic. For example, the rectangular model would require $\beta = 3.65$. The results of *Minnis and Wielicki* [1988], though not necessarily representative of the situation here, show no indication of algorithm bias, although that is a more plausible explanation. Further study is required to resolve this problem with small amounts of low cloudiness. For the present, it is assumed that the data are accurate. In the absence of a more accurate physical model for the very small cloud amounts, values of $\gamma_k > 1.0$ are used here but are limited to values less than or equal to 2.

6.3. *Total Cloudiness*

Negative coefficient values in (17) lead to an increase in the masking effect so that with increasing VZA there is a smaller change in the lower level cloud amounts than expected for the single-layer case. The vertical proximity of the cloud layers may determine whether the exposure is greater than the masking when the VZA changes. For example, raising the lower cloud in Figure 1*f* increases its exposure at θ, while the opposite is true if it is lowered. Thus the relative heights of the cloud layers should play an important role in the amount of lower level cloudiness which is obscured as the VZA increases. This may help explain the relative values of b_i. The obscuration effect of midlevel clouds over low clouds is about one third that of high clouds over low clouds. Values of the coefficients for the middle- and high-cloud overlap fall between the other two, consistent with the relative heights of the cloud layers.

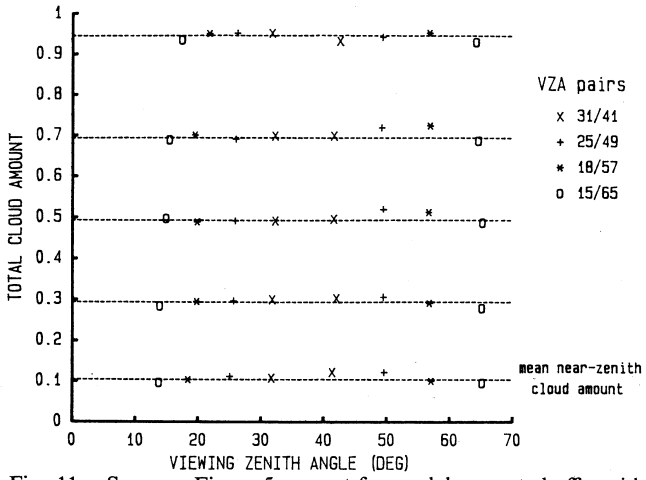

Fig. 11. Same as Figure 5, except for model-corrected off-zenith cloud amounts.

Table 6 shows that, on average, the model provides a good fit to the observed changes in total and layer cloudiness with VZA. To determine how the model performs for individual VZA pairs, the resultant mean total cloud amount pairs are plotted in Figure 11. Figure 11 may be compared to Figure 5. The model significantly reduced the bias for all angular pairs, except for those in which the cloud amount decreased with increasing VZA. It also failed to account for all of the variations in the VZA–cloud amount curves. Specifically, the corrections at $\theta \approx 50°$ underestimate the VZA effect, while those at $\theta \approx 65°$ usually overcompensate for the influence of the VZA. The data in Figures 5 and 7 suggest that the dependency of cloud amount on VZA may not be monotonic. The Student t tests mentioned in section 5.2 indicate that the tendency for some mean cloud amounts to decrease for $\theta > 60°$ is statistically insignificant. The lower values of cloud amount in those bins is probably caused by sampling biases in the data. Since the angular bins are tied to certain geographies as a result of the GOES viewing geometry (see Figure 3), it is possible that the types of clouds observed at $\theta > 60°$ are different than those observed at $\theta < 60°$.

6.4. *Applications*

6.4.1. *Model applications.* If the true cloud amount is known, application of the model is straightforward. The variations of single-layer cloudiness with VZA are shown in Figure 12 for low, middle, and high clouds. These results are based on the values γ_k in Figure 9 used in (16). The curves reflect the values of the masking exponents and the data in Figure 7. The high clouds increase more at greater cloud amounts than low and midlevel clouds. At small cloud amounts, low-cloud cover increases more rapidly with VZA than the other cloud layers.

Whenever cloud cover is known for one VZA and desired at another, the "true" cloud cover, C_0, must be determined initially. This is accomplished by taking the observed values of C_2, C_3, and C_4 and computing C_{0_2}, C_{0_3}, and C_{0_4}. The latter is determined first by solving (16) iteratively for the highest cloud layer. Consider an observation of a cloud field containing three layers. An initial guess of C_0 (usually the observed value) is made to select γ_4, which is used to compute C_4* with (16). This intermediate value is compared

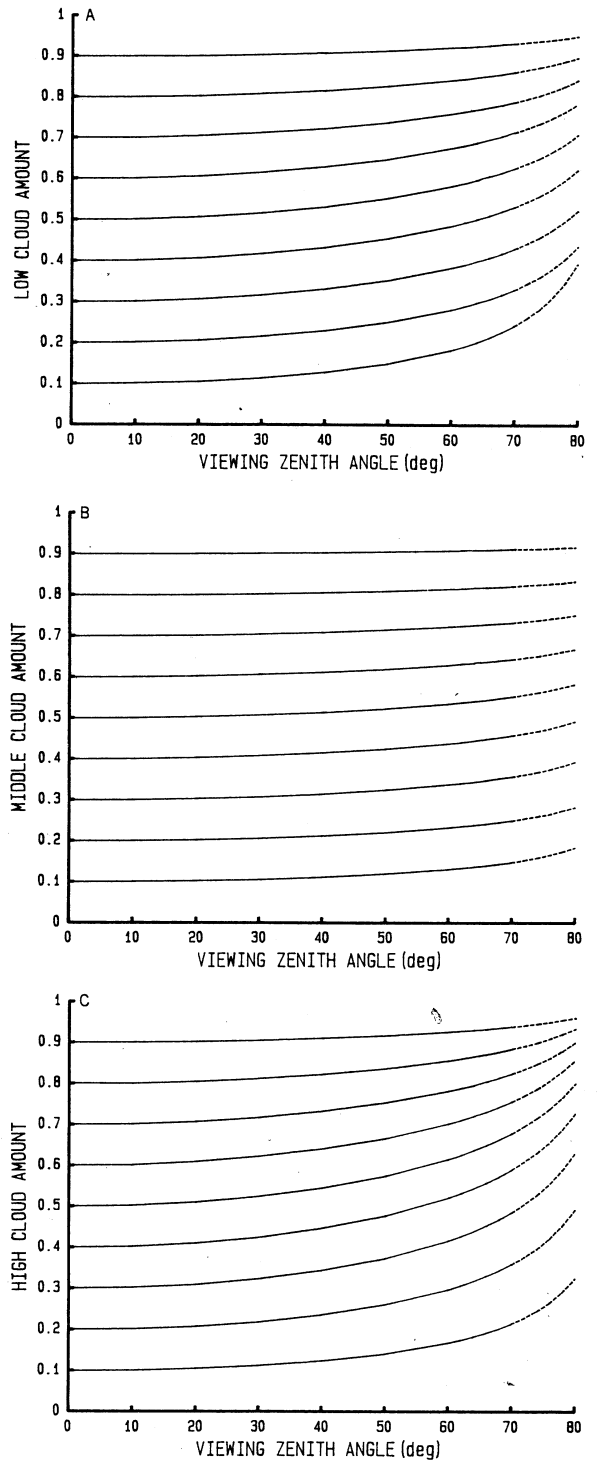

Fig. 12. Variation of single-layer cloudiness with viewing zenith angle using fitted cumulus model for (*a*) low, (*b*) middle, and (*c*) high clouds.

to the observation in order to make a new guess of C_{0_4}. When $C_4 = C_4$*, the correct value of C_{0_4} has been obtained, and the iteration ceases. The value of $C_4' = C_4$, since there is no obscuration of C_4. After dividing C_3 by $(1 + b_3 C_4' \tan \theta)$, C_{0_3} is determined by following the iterative procedure outlined above. The value of C_{0_3} is then used in (16) to compute C_3'. Nadir cloud amount for the lowest layer follows the same procedure as that for C_3, except that C_2 is divided by $\{1 + [b_1 C_3' + b_2 C_4'] \tan \theta\}$. Equation (17) can then be solved for

any angle θ, since the values for the masking exponents and nadir cloud amounts are known. If only low and midlevel clouds are present, $C_3' = C_3$, since no high clouds are obscuring midlevel clouds. For a single-layer case, all terms involving b_i reduce to zero.

An example of this process is illustrated below; using some of the actual data. Given $C_1 = 0.636$ measured at $\theta = 56°$, a value of $C_1(\theta_n)$ is required where $\theta_n = 37°$. $C_2 = 0.198$, $C_3 = 0.293$, and $C_4 = 0.145$. Applying the process described above yields $\gamma_4 = 0.628$, $C_{0_4} = 0.091$, and $C_4(\theta_n) = 0.110$. Because of obscuration, $C_3' = 0.301$ initially. From iteration, $\gamma_3 = 0.146$, $C_{0_3} = 0.270$, and $C_3(\theta_n) = 0.280$. The initial value of $C_2' = 0.217$, yielding $\gamma_2 = 0.502$, $C_{0_2} = 0.149$, and $C_2(\theta_n) = 0.174$. Summing these values yields $C_1 = 0.564$.

There are some basic limitations to the model which must be taken into account in any application. Total cloud cover is always constrained between 0 and 1. If the observed total cloud cover is 0 or 1, then the corrected cloudiness is forced to remain equal to the observed value. For a single-layer cloud field, this constraint is automatic, since the values of γ are zero at $C = 1$. For a multilayer cloud field with $C_1 = 1$, however, this constraint is not automatic (that is, a value of $C_1(\theta) \neq 1$ may be computed) using (17). An external means is required to enforce this constraint. This is accomplished in the following manner. The layer cloud amounts are adjusted for θ, using (17) in the usual fashion. If $C_1 = 1$, but $C_{0_1} < 1$, then the zenith amounts of the lower-level clouds are reduced in proportion to their relative amounts, such that $C_{0_1} = 1$. It is also possible to obtain values of $C_1(\theta) > 1$ using (17), when θ is increased. Whenever $C_1(\theta) > 1$, the amounts of lower-level clouds are reduced in proportion to their relative amounts, such that $C_1(\theta) = 1$. In both situations the cloud amount in the highest layer is always permitted to vary with θ according to (16), while the lower-level cloud amounts are adjusted to force the total cloud amount to unity.

This methodology was applied earlier to estimate by how much the bias errors due to VZA effects may be reduced. Off-zenith cloud amounts were converted to "true" cloud amounts and then used to predict the cloud amount at θ_n. Differences were computed between the observed near-zenith cloudiness and the corrected off-zenith cloud cover. The results are shown in Tables 5 and 6 and Figure 11.

6.4.2. *Satellite-derived cloudiness.* This model was applied to the 15-day, 3-hourly cloud data set derived by MHG over a region centered at 13.8°N and 133.8° to illustrate how the VZA effect may bias the derived mean cloudiness. These data were originally taken at $\theta \approx 14°$, so that they are assumed to constitute a realistic "true" cloud data set. The cloud amounts were adjusted to several values of θ and were averaged to simulate various positions of a geosynchronous satellite. A Sun-sychronous satellite sampling pattern was also simulated for a VZA range from 0° to 70°. This pattern was applied in the same fashion for all eight local times to ensure that the results would be consistent for all local hours. Nine different starting VZAs were used to derive nine 15-day means. These means were then averaged to arrive at values which are independent of the starting VZA. It was assumed that the cloud amounts derived using IR-only data have the same VZA dependence as those derived from data taken at $\theta < 81°$.

Results of this simulation are shown in Figure 13. This region is dominated by low stratocumulus and trade cumulus clouds which have a substantial diurnal variation. It is

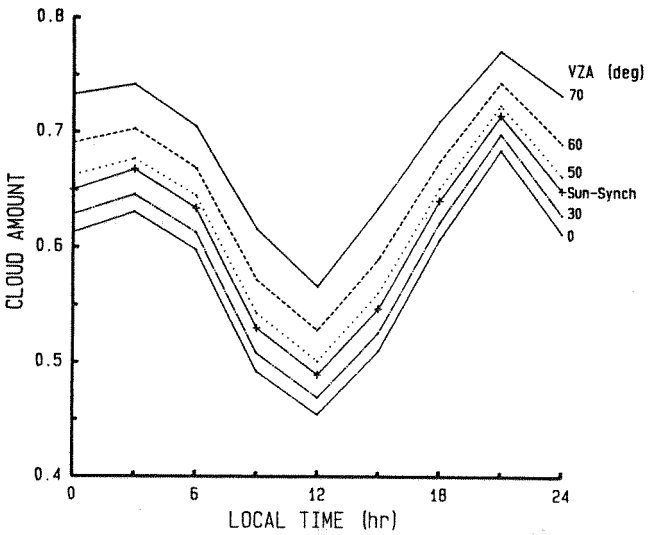

Fig. 13. Simulation of observed mean total cloudiness for a 2.5° × 2.5° region at 13.8°N and 133.8°W during July 17–31, 1983, for various viewing zenith angles and an average Sun-synchronous sampling.

apparent that the VZA changes affect the relative diurnal variations only slightly, decreasing the diurnal range from 0.231 to 0.206 at $\theta = 70°$. At $\theta = 30°$ the bias in the period mean is 0.015, increasing to 0.047 at $\theta = 50°$. The maximum bias of 0.111 is found for $\theta = 70°$. The bias found for the Sun-synchronous satellite, 0.036, is equivalent to that for $\theta \approx 45°$. These are substantial errors relative to the ISCCP goal of deriving the monthly mean cloud amount to an accuracy of ±0.03 [*Schiffer and Rossow*, 1983]. While this single example does not necessarily represent the global mean conditions, it clearly shows that the effect of the satellite zenith angle cannot be ignored in the construction of a well-sampled global cloud data set.

6.4.3. *Limitations.* Any application of the VZA dependent cloud cover model developed here must consider its limitations. The coefficients and exponents have been derived for $\theta < 71°$ and hence may be unreliable for greater VZAs. The values for the model parameters were computed from mean cloudiness over a particular oceanic area and may not be representative of the dependence of mean cloud cover on VZA in other regions. When used for individual measurements, the deviations of the model parameters from mean conditions must be taken into account. For example, Tables 5 and 6 show that the average standard deviations about the mean differences are around 0.11, while Figure 6 indicates that these deviations increase with VZA. If it is assumed that deviations due to the algorithm, relative azimuth angle, and sampling are 0.07 (Table 1), then the average standard deviation due to changes in VZA is ≈0.08. Values of γ and b have been derived for both the nominal HBTM results and for resolution-corrected data. Thus if a different method is used to derive cloud fraction and its dependence on pixel resolution is known, the latter data may be used, assuming that they are representative of the perspective effects on observed cloud cover.

7. CONCLUDING REMARKS

A set of satellite-observed cloud amount data taken over the tropical Pacific Ocean have been analyzed to derive the

mean dependence of cloud amount on the viewing zenith angle. This relationship was found to be a function of cloud type and amount. The changes in observed cloud fraction due to VZA can be as great as 110% for VZAs as high as 71°. Geometrical effects appear to be the predominant reason for the marked increase of cloud cover with increasing VZA. In some cases, up to 28% of the increases may be attributed to the degraded pixel resolution at higher VZAs. The results were fitted to several different idealized geometrical cloud models. It was determined that a single-layer cumulus model which relies on a single parameter, the masking exponent, provided the best fit to the single-layer data. Although only qualitative evaluations are possible at this time, the variations of the values of the masking exponent with cloud layer appear to be quite consistent with the types of clouds usually found in the defined layers. An additional formulation was derived to describe the VZA dependence of total cloud cover for various mixes of low-, middle-, and high-cloud cover in terms of their single-layer model parameters. Application of these models to the off-zenith angle cloud amounts reduced the mean differences between the individual off-zenith and near-zenith cloud amounts from 0.054 to 0.004. The model coefficients were determined for HBTM cloud amounts and therefore are not necessarily the same as those which would be derived from cloudiness analyzed with other algorithms.

It is clear from this study that the variation of cloudiness with the viewing angle is an important consideration in cloud cover quantification. Comparisons of model-derived cloud fractions with observations will need a reference point such as the "true" cloud fraction used here. Either the observations must be normalized to the reference, or the computed cloud amounts must be adjusted to the observation angles. Simulations of cloud cover for Earth observation applications must also consider this aspect of viewing. Calculations of radiative transfer through the atmosphere may need to incorporate VZA effects in order to achieve higher degrees of accuracy. Despite sampling and geographical limitations, the model developed here provides a simple, realistic means for accounting for these effects in the quantification of cloud cover. Future research will help determine if these effects vary substantially with cloud algorithm, geographical location, and season.

APPENDIX

Single Cloud Models

Derivations of the idealized cloud models given in section 2 are found in the report by J. W. Snow and D. D. Grantham (Variation of cumuliform cloud amount with angle view, *AFGL Technical Report* in preparation, 1989). Those derivations are briefly reviewed below considering only single clouds, so that $\gamma = 1$.

The spherical model assumes that the cloud is a sphere, with radius r. The cloud area is $C = 2\pi r$, and the effective aspect ratio is unity. Projection of the sphere onto a surface at zenith angle θ yields (2). The hemispherical dome is derived by treating the cloud by portions. The half of the hemisphere toward the observer always appears as half of a horizontal disk, $C/2$, while the other half cuts the view as a halved hemisphere, or C sec $\theta/2$. Combining these parts gives (3). A hemispherical domed cylinder consists of a hemisphere of radius r resting on a cylinder of radius r and height z. The thickness parameter of the cylindrical portion of the cloud is $B = 8\beta_c/\pi$, where $\beta_c = z/2r$. Placing the cylinder under the hemisphere results in the addition of CB tan $\theta/2$ to (3), yielding the formulation in (4).

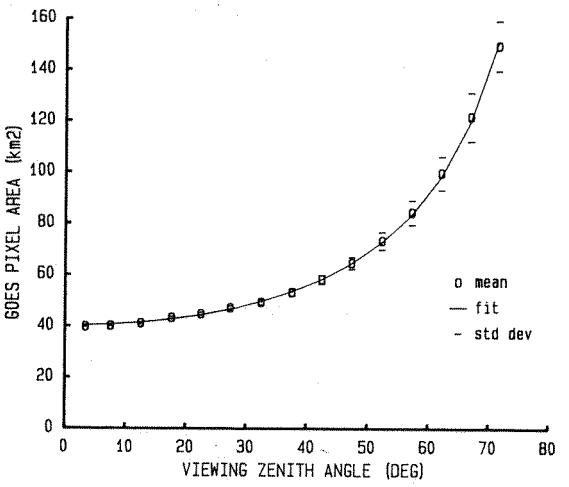

Fig. A1. Estimation of areal coverage at Earth's surface for GOES 6 8-km pixel.

The hemispherical dome appears to be a reasonably realistic model of cumulus clouds, but it suffers two shortcomings for interpreting real cloud fields. The thickness parameter must be known or specified, and $dC/d\theta \neq 0$ at $\theta = 0$. Both weaknesses may be eliminated by using a modification of (4), the single-layer cumulus model. This modification is accomplished by taking the derivative of (4), substituting a series approximation to the resulting trigonometric function, setting it equal to zero, and solving for B. If only the first-order term is retained in the series approximation of sin θ, two solutions are obtained for B: $B = 0$ and $B = -\theta$. Since sin θ is positive for $0 < \theta < \pi$ and a positive value is required here, $B = |\theta|$. The trivial solution reduces (4) to (3), while the latter value of B results in (5). This simple solution satisfies the derivative criterion but does not require any thickness parameter specification.

GOES Pixel Area Versus VZA

Several approaches may be taken to determine the change in the effective area of a GOES pixel with VZA. One method is to take the number of pixels which are navigated into a box of known area and to compute the average area per pixel for boxes at various θ. In this study an area of ±50° of latitude and longitude from the satellite subpoint was divided into 2.5° regions. The area of each region depends only on latitude. All of the GOES pixels which corresponded to points within this area were navigated as in the work by MHa for one VIS–IR image and summed into their respective 2.5° regions. The value of θ was determined for the center of each region. The resultant pixel area for each region was then summed into VZA bins of 5°. An average pixel area and VZA were found for each VZA bin, using the values from 1600 regions. The means and standard deviations for GOES 6 are shown in Figure A1. Standard deviation increases with increasing θ. It was determined from linear regression that the average pixel areas could be represented with a rms error of less than 1% with (9*b*) for $\theta \leq 72$. This approximation, shown as the solid line in Figure A1, is sufficient for the purposes of this study.

Acknowledgments. The assistance of G. Gibson and P. Heck of Planning Research Corporation in the preparation of the figures and of Sara Eckhaus of Computer Sciences Corporation in the reduction of the data is deeply appreciated. Discussions with J. W. Snow, Air Force Geophysics Laborabory, concerning the analytical model for single-layer cumulus cloud cover were also quite helpful.

REFERENCES

Bunting, J. T., and K. R. Hardy, Cloud identification and characterization from satellites, in *Satellite Sensing of a Cloudy Atmosphere; Observing the Third Planet*, edited by A. Henderson-Sellers, pp. 203–240, Taylor and Francis, London, 1984.

Hahn, C. J., S. G. Warren, J. London, R. M. Chervin, and R. Jenne, Atlas of simultaneous occurrence of different cloud types over the ocean, *NCAR/TN-201+STR*, 212 pp., Natl. Cent. for Atmos. Res., Boulder, Colo., 1982.

Jacobowitz, H., H. V. Soule, H. L. Kyle, F. B. House, and the Nimbus 7 ERB Experiment Team, The Earth Radiation Budget (ERB) Experiment: An overview, *J. Geophys. Res.*, *89*, 5021–5038, 1984.

Kuettner, J. P., Cloud bands in the Earth's atmosphere, *Tellus*, *23*, 404–426, 1971.

Lund, I. A., and M. D. Shanklin, Universal methods for estimating probabilities of cloud-free lines-of-sight through the atmosphere, *J. Appl. Meteorol.*, *12*, 28–35, 1973.

Malberg, H., Comparison of mean cloud cover obtained by satellite photographs and ground-based observations over Europe and the Atlantic, *Mon. Weather Rev.*, *101*, 893–887, 1973.

Minnis, P., and E. F. Harrison, Diurnal variability of regional cloud and clear-sky radiative parameters derived from GOES data, I, Analysis method. *J. Clim. Appl. Meteorol.*, *23*, 993–1011, 1984*a*.

Minnis, P., and E. F. Harrison, Diurnal variability of regional cloud and clear-sky radiative parameters derived from GOES data, III, November 1978 radiative parameters. *J. Clim. Appl. Meteorol.*, *23*, 1032–1051, 1984*b*.

Minnis, P., and B. W. Wielicki, Comparison of cloud amounts derived using GOES and Landsat data, *J. Geophys. Res.*, *93*, 9385–9403, 1988.

Minnis, P., E. F. Harrison, and G. G. Gibson, Cloud cover over the eastern equatorial Pacific derived from July 1983 ISCCP data using a hybrid bispectral threshold method, *J. Geophys. Res.*, *92*, 4051–4073, 1987.

Rossow, W. B., et al., ISCCP cloud algorithm intercomparison, *J. Clim. Appl. Meteorol.*, *24*, 877–903, 1985.

Schiffer, R. A., and W. B. Rossow, The International Satellite Cloud Climatology Project (ISCCP): The first project of the World Climate Research Programme, *Bull. Am. Meteorol. Soc.*, *64*, 779–784, 1983.

Shenk, W. E., and V. V. Salomonson, A simulation study exploring the effects of sensor spatial resolution on estimates of cloud cover from satellites, *J. Appl. Meteorol.*, *11*, 214–220, 1972.

Snow, J. W., Field of cumuliform clouds east of Cape Canaveral, Florida, *Eos Trans. AGU*, *67*, 595, 1986.

Snow, J. W., J. Bunting, R. d'Entremont, D. Grantham, K. Hardy, and E. Tomlinson, Space shuttle cloud photographs assist in correcting meteorological satellite data, *Eos Trans. AGU*, *66*, 489–490, 1985.

Snow, J. W., D. D. Grantham, E. M. Tomlinson, and J. H. Willand, The characterization of cumuliform cloud fields using space shuttle photography, paper presented at Conference on Satellite Meteorology and Remote Sensing, Am. Meteorol. Soc., Williamsburg, Va., May 13–16, 1986.

Vemury, S. K., L. Stowe, and H. Jacobowitz, Sample size and scene identification (cloud): Effect on albedo, *J. Geophys. Res.*, *89*, 5345–5353, 1984.

P. Minnis, Atmospheric Sciences Division, MS 420, NASA Langley Research Center, Hampton, VA 23665.

(Received March 29, 1988;
revised September 15, 1988;
accepted November 2, 1988.)

data were filtered for obvious navigation and extreme misclassification errors by removing all data pairs having $C(\theta_f)_1 - C(\theta_n)_1 > 0.45$ and $C(\theta_f)_1 - C(\theta_n)_1 < -0.25$. This somewhat crude filter removed about 3% of the data. Its asymmetric constraints were established by combining an assumed mean VZA bias of 0.10, a maximum $\sigma = \pm 0.18$ computed from an initial processing of the data, and an error of ± 0.17, resulting from potential navigation errors as great as a three-pixel shift (for an overcast region surrounded by clear regions). This filter had little effect on well-sampled bins, but its eliminated a few sparsely sampled bins from the results.

A single-layer cloud field is defined here as a layer containing clouds with no significant cloudiness above it. Thus additional limits were set arbitrarily for the acceptance of single-layer cloud amounts, in order to minimize interference by clouds higher than the specified cloud layer. For midlevel clouds, $C(\theta_n)_3$ is used only if

$$C(\theta_n)_3 / \{C(\theta_n)_3 + C(\theta_n)_4\} > 0.99$$

Low clouds are accepted only if

$$C(\theta_n)_2 / C(\theta_n)_1 > 0.99$$

These constraints allow a maximum of 0.01 detected cloud cover above the specified cloud layer. Although there may be some upper level cloudiness misclassified as lower level clouds because of partially filled pixels, these limits should minimize their influence on lower level cloud amounts.

4.1. *Model Analysis*

4.1.1. *Single-layer cloud fields.* If there is a VZA dependency in C between θ_0 and any other θ, then it is probable that the near-zenith mean cloud amounts computed for angular bins $i = 1, 4$ for a given cloud amount range do not necessarily correspond to the same cloud fraction at θ_0. On the basis of the slight change in cloudiness with θ for $\theta < 40°$ in this (as will be seen in section 5) and other studies [e.g., *Snow et al.*, 1986], it is assumed that the true cloud amounts are sufficiently close that the VZA relationships to cloudiness for $i = 1, 4$ are nearly equal for all $\bar{\theta}_n$. It is possible, then, to estimate the VZA dependency of cloud cover for a given cloud amount and type by determining the mean relationship of C to θ for all four angular bins. The dependencies are derived in terms of the simple models given by (1)–(5), since $\bar{C}(\bar{\theta}_n)_{ijk}$ and $\bar{C}(\bar{\theta}_f)_{ijk}$ should be equal at θ_0.

For example, from (2)

$$\bar{C}_{0_{ijk}} = \bar{C}(\bar{\theta}_n)_{ijk} / \sec^{\gamma}(\bar{\theta}_n)_{ijk} \tag{12a}$$

and

$$\bar{C}_{0_{ijk}} = \bar{C}(\bar{\theta}_f)_{ijk} / \sec^{\gamma}(\bar{\theta}_f)_{ijk} \tag{12b}$$

As suggested by *Snow et al.* [1986], the logarithms of (12) can be rearranged to yield

$$\gamma_{ijk} = \ln [C(\theta_n)/C(\theta_f)] / \ln [\sec \theta_n / \sec \theta_f] \tag{13a}$$

The masking exponent is determined in a similar fashion for all of the other models given by (2) through (5). Setting $\gamma = 1$, the effective aspect ratio in (1) may be given by

$$\beta_{ijk} = \{[C(\theta_n) - C(\theta_f)] / [C(\theta_f) \tan \theta_n - C(\theta_n) \tan \theta_f]\} \tag{13b}$$

The indices and overbars have been omitted in (13) for clarity.

A mean masking exponent,

$$\bar{\gamma}_{jk} = \sum_{i=1}^{4} \gamma_{ijk} N_{ijk} / \sum_{i=1}^{4} N_{ijk}$$

or aspect ratio, is then computed for each cloud type and cloud amount category. The mean cloud amounts at zenith are then computed for the near-and-off-zenith cloud fractions from each cloud amount pair, using each model and its corresponding value of $\bar{\gamma}_{jk}$. The mean and rms differences between the pairs of zenith cloud amounts normalized to the average predicted zenith cloud amounts are computed for each category jk and used to assist in the evaluation of the models. The values of $\bar{\gamma}_{jk}$ for the selected model are then used to graphically estimate $\bar{\gamma}_k$ for all cloud amounts.

4.1.2. *Total cloudiness.* The selected single-layer model is substituted into (7) yielding a more explicit formula for total cloud cover. The coefficients, b_i, are determined by multiple regression on the individual pairs of near-zenith and off-zenith total cloud amounts which are comprised of more than one layer. Thus remaining individual layer cloud amount pairs which were not used in determining values of γ_k, for $k = 2, 4$, in section 4.1.1 are included in this analysis. In order to perform the regression, it is necessary to assume that the interlayer obscuration is negligible for the near-zenith VZAs. This enables the determination of single-layer cloud amounts at θ_0 from the near-zenith, single-layer cloud amounts. The values of $C(\theta_f)_1$ are regressed with the corresponding values of $C_{0_k}(k = 2, 4)$ derived from the near-zenith, single-layer cloud amounts.

4.2. *Resolution Effects*

The contribution of degrading resolution to the change in cloud amount with VZA is estimated by computing the mean differences between the pairs of C_E and C_S in each category jk, using the values of C_E to determine the cloud amount category. Assuming that the change in cloud amount is linear with pixel area, the average change in cloud cover for a given mean cloud amount pair, $\bar{C}(\bar{\theta}_n)_{ijk}$ and $\bar{C}(\bar{\theta}_f)_{ijk}$, due to change in resolution is

$$\Delta C_{Rijk} = P_{jk} \bar{C}(\bar{\theta}_n)_{ijk} \{A(\bar{\theta}_f) - A(\bar{\theta}_n)\} / \bar{A}(\theta_n) \tag{14}$$

where $P_{jk} = (\bar{C}_{Sjk} - \bar{C}_{Ejk}) / 3\bar{C}_{Ejk}$. The factor of 3 in the divisor of this equation is the value of the areal term as given in (14). It represents the fourfold increase in pixel area between 8-km and 16-km GOES data, with the pixel area, A given by (9). The value of the off-zenith cloud amount is then corrected to account for the resolution change by

$$\bar{C}_R(\bar{\theta}_f)_{ijk} = \bar{C}(\bar{\theta}_f)_{ijk} - \Delta C_{Rijk} \tag{15}$$

where the subscript R denotes resolution correction. These corrected quantities are then analyzed with their corresponding values of $\bar{C}(\bar{\theta}_n)_{ijk}$ following these procedures.

4.3. *Other Considerations*

Using different satellites to provide the VZA pairs over a given region introduces the possibility of variations in cloud cover due not only to VZA differences, but also to temporal, azimuthal, and instrumental differences as well as algorith-